Characterising the Lightning Source for the MTG Lightning Imager Mission

Final Report

EUM/MTG/SOW/05/0028

Technical Report

Ullrich Finke

Institut für Meteorologie und Klimatologie

Universität Hannover

2. June 2006

Contents

1 Introduction

For the next generation of geostationary earth observation satellites (Meteosat Third Generation - MTG) an optical Lightning Imaging (LI) mission is planned. The aim is to observe permanently the lightning activity and provide the lightning location data with accuracy of 10 km and detection efficiency of 90%. These continuous lightning data for the whole hemisphere would represent a new data set for use in a manifold of applications in nowcasting, climatology and atmospheric research.

The instrument studies for the lightning imager need as input the characteristics of the lightning source. A large number of ground based lightning detection systems are in operation currently. However these systems detect the radio emissions from lightning, while optical observations are rare. There exist only few observations with optical instruments from aircraft (Christian and Goodman, 1987; Mach et al., 2003). Recently a huge data source has become available from the optical lightning observation from low orbit satellites with the LIS and OTD instruments.

The present study will analyse these data sets and give a statistical description of the lightning source with respect to its temporal, spatial and radiation characteristics. Additionally a simple Monte-Carlo simulation model of the radiation transfer from a lightning source through the cloud up to the cloud surface will be developed. This model can be used for studying the impact of various parameters of the lightning source and cloud parameters to the upwelling radiation which can be observed from space.

2 The LIS and OTD data sets

2.1 Instrument description

Since the mid of the 1990s NASA operates 2 lightning detection sensors on board of low orbit satellites. Both instruments - the OTD (Optical Transient Detector) and LIS (Lightning Imaging Sensor) - and the detection algorithms are described in detail by Christian et al. (1989, 2003); Boccippio et al. (2000). Lightning is detected by its optical radiation at 777.4 nm with a CCD-matrix. In order to discriminate the lightning signal from the bright background of illuminated clouds a narrow filtering with respect to wavelength and time is applied. Additionally an elaborated on-board real time event processing algorithm was implemented which detects the transient lighting signal from the slowly changing background.

The relevant parameters of both instruments are summarized in Table 1.

2.2 Data set description

2.2.1 Data content

The available data sets cover an observation time of 5 years (OTD) and 7 years (LIS). The data contain position, time and radiation amplitudes of each detected lightning event.

The sensor pixels detect the *energy* which is collected during the time frame of 2 ms which was filtered in a narrow bandwidth filter $\Delta\lambda$. Hence the radiance data are given in units of $\mu\mathrm{J\,ster^{-1}\,m^{-2}\,\mu m^{-1}}$

	OTD	LIS
pixel array	128x128	128x128
pixel resolution	3-6 km	8-13 km
total FOV	1300 km×1300 km	550 km×550 km
location viewtime	1-270 s	90 s
single frame integration time	2 ms	2 ms
detection efficiency	50%	90%
attitude stability	changing	very high

Table 1: Parameters of the OTD and LIS sensors.

The filter width $\Delta\lambda$ is $8.59 \cdot 10^{-10}$m (OTD) resp. $9.09 \cdot 10^{-10}$m (LIS). This filter width must be multiplied to the radiance values in the data set in order to get the quantity in usual units of μJ ster^{-1} m^{-2}.

The data sets also contain background images in the considered spectral window. These background images were taken in $\sim$ 35 sec time intervals and are available in separate data files. For each detected event a value for the background radiation is given which is estimated from the background image closest in time or from the solar zenith angle.

2.2.2 Data organisation

The structure of the data set is given in detail in Boccippio et al. (1998). A brief description of the parts relevant for this study is given in the following.

Basically the data represent point data indicating the energy which was detected by a single pixel in a certain time interval. Using the orbit geometry and sensor attitude the geo-position is calculated. These elementary events are organized into a parent-children *hierarchy* of events, groups, flashes and areas (for details cf. Christian et al., 1995).

Event A single pixel's radiation energy accumulated during the time frame (2ms) exceeded the threshold. The event is characterised by its radiance, time, geolocation and footprint.

Group Adjacent events in one time frame. This is assumed to be associated with a single discharge process, such as a lightning return stroke or an intracloud recoil streamer.

Flash Collection of groups close in time and space constitute a flash. Lightning flashes also consists typically of few single return strokes separated by 50-300 ms.

Area Collecting flashes into a common area which is assumed to represent a storm. This item is not used in the presented analysis.

For all these items the location, time, radiance is given as well as the relation to the constituting children (pointer and count) and the associated parent item (pointer). Throughout this study we will follow the terminology as used in the data set. For reference the translation of the relevant termini into physical and meteorological phenomenons is given in the Table 2.

We note that the MTG mission requirements refer to lightning strokes and flashes, i.e. correspond to groups and flashes in the LIS-data.

Data set term	Physical quantity
event	single CCD-pixel received energy above the threshold
group	lightning optical pulse produced by the return stroke in cloud-to-ground lightning or the recoil streamer in intra-cloud lightning
flash	lightning flash, consisting of several strokes
footprint	area of the pixels onto the ground (or cloud surface)
radiance	energy per time, solid angle and area

Table 2: Translation of the termini used in the data set into the corresponding physical quantities.

Additionally the data set contains summary data for orbit and for seconds as well as orbit meta data and status information. The data are organised in HDF-files for each orbit.

An example of the lightning location data for the orbits of one day is given in Figure 1.

3 Method of the analysis

3.1 Data selection and preparation

The complete available data set was obtained from NASA. It contains 7 years LIS-data and 5 years of OTD-data. The data are organized in single HDF-files per orbit. For access of the data a software library in IDL (Interactive Data Language) is available (Boccippio et al., 1998). Basing on this library the software for the following statistical analysis was written in IDL.

3.1.1 Instrument and time period

The LIS instrument was selected for the data analysis due to its higher attitude stability and the higher resolution and detection efficiency (see Sec. 2, table Table 1).

The whole LIS data set spans over 7 years. In order to speed up the calculations a subset in time was used: the year 2004, were the instrument was working with high reliability and quality. Various tests on the data were performed in order to assure that the data from the other years show the same statistical behaviour.

3.1.2 Data quality

The purpose of the presented study is to characterise the *lightning source*, hence the data with maximum quality were selected. This was realized by a filtering of the whole data set with the following 3 filters. For each of the analysed quantity it will be indicated which of the filters was applied.

Local solar time Optical lightning detection is affected by the non-lightning background illumination due to the solar insulation. For the characterisation of the lightning signal alone the best optical conditions for lightning observation were selected. Thus, in order to avoid any influence from the

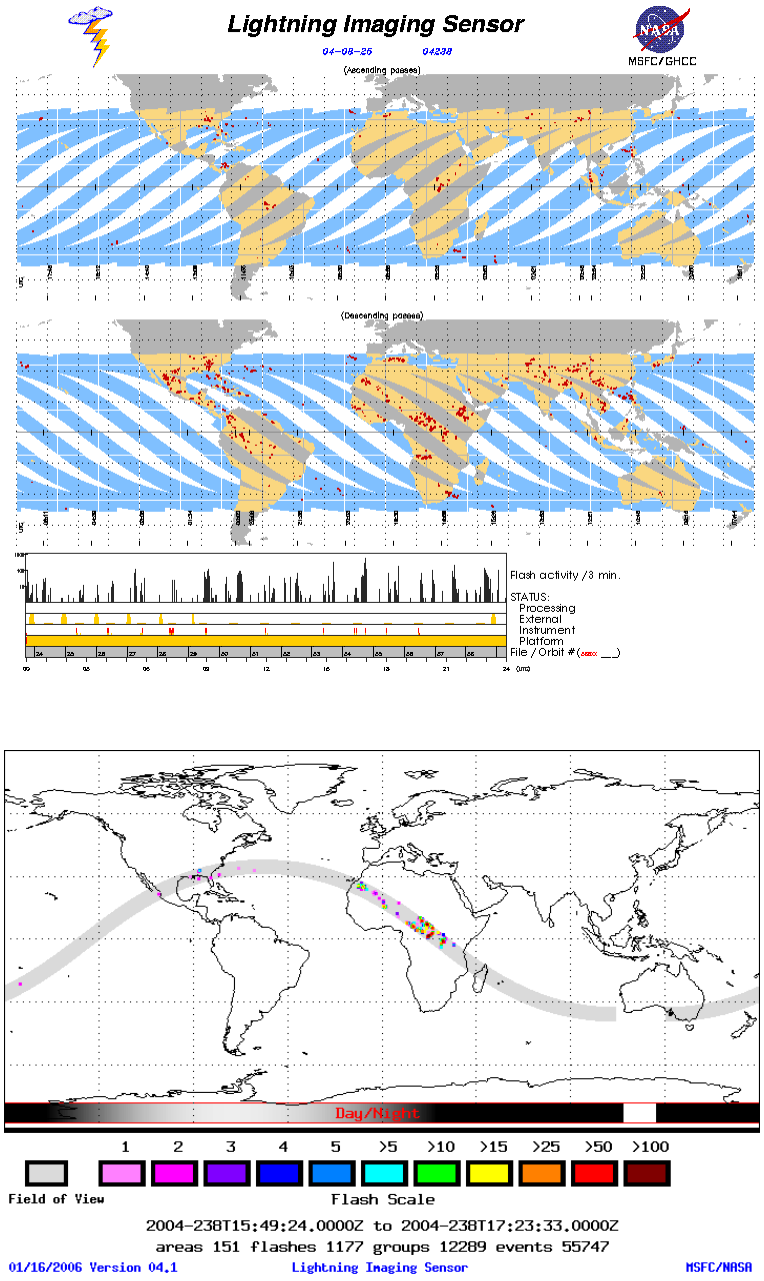

Figure 1: Lightning position data detected by the LIS for the 16 orbits of the 25.8.2004 (top) and for a single orbit (bottom) (http://thunder.msfc.nasa.gov/data/lisbrowse.html)

background radiation only the night-time data during 20 - 04 Local Solar Time (LST) were extracted for the analysis.

Both day and night data were used, however, for the characterisation of the background radiation and the signal to noise ratio between lightning and the background (Sec. 8).

Central pixels Boccippio et al. (2002) describe for the various performance parameters the de-

pendency on position on the CCD-array. The center of the array is pointed into the nadir direction (boresight direction). With increasing off-boresight angle a degradation in detection efficiency and an enhancement of the ground footprint of the pixels is observed due to geometrical and optical reasons. Hence for the analysis presented here only the central pixels ± 30 (for radiation data), resp. ± 50 (for temporal and spatial analysis) were used.

Alert flags The data contain alert flags which indicate error in data and warning conditions from various reasons. Only data without any alert indication were used for this analysis.

3.1.3 Data organisation

The classification into groups, flashes were used as found, no attempts were made to create a new classification. The following analyses focus mainly on groups (lightning strokes), since they represent the elementary lightning event. In order to speed up the data processing the events, groups and flash data per orbit were re-saved in separate binary files.

3.2 Data analysis

3.2.1 Parameters

This study will focus on the statistical analysis of parameters which are most relevant for sensor instrument studies. Therefore, we will not present here the various climatological and meteorological statistics of the global distribution of lightning with its annual and diurnal cycle. These analyses can be found in a number of publications (e.g. Christian et al., 2003).

The data analysis was performed for the following key parameters:

Temporal Characteristics The time series observed inside the field of view of the LIS instrument has been analysed. These data then have to be extrapolated onto the entire visible disk. The aim is to derive an estimate of frequency of lightning and the duration of entire lightning flashes consisting of several groups.

Spatial Structure The footprint size of lightning events and groups was analysed. This estimates the spatial size of the lightning strokes as seen from an observer above the clouds. Furthermore the number of events which are detected during a single time frame of 2 ms is analysed.

Radiation Lightning radiance per pixel is stored in the data. The minimum detectable radiation is 3 $\mu\mathrm{J\,m^{-2}\,sr^{-1}}$, the maximum is 500 $\mu\mathrm{J\,m^{-2}\,sr^{-1}}$. One has to be aware of saturation effects in the group data (total over constituting events), which underestimate the highest radiation amplitudes.

Background radiation The background radiation is analysed using the LIS background radiation data and additionally the data from cloud observation satellites (Meteosat). The LIS data contain the background images, which are available approximately for every 35 seconds. Additionally, for each detected event (pixel) the corresponding background illumination derived from the background images is contained in the event data. The data associated to the events were used in the first step and are presented here.

The background radiation data together with the lightning radiances will be used to estimate the *signal to noise ratio* under day and night condition.

3.2.2 Data presentation

Many of the results are presented in form of normalized histograms, i.e. distribution functions, in some cases accompanied by the cumulative distribution. These empirical frequency distribution density functions were calculated as follows:

Originally the data are provided as discrete values of the corresponding quantities $R_i, t_i, \gamma_i, \dots$ such as radiance, longitude, latitude, time...

The frequency distribution of the quantities is calculated as 'histogram' for a certain bin size (e.g. ΔR) between minimum and maximum values. This frequency distribution function can be expressed as:

$$N(R_k, \gamma_j, \dots) = \sum_i \delta(R_i - R_k)\delta(\gamma_j - \gamma_i) \cdots \tag{1}$$

where the discrete data $(R_i, \dots)$ now indicate the data binned in classes corresponding to the bin size.

>From this function the distribution for one single quantity is calculated:

$$N(R_k) = \sum_{j,\dots} N(R_k, \gamma_j, \cdots) \tag{2}$$

The distribution can be weighted according to some parameter γ, e.g. the viewtime:

$$M(R_k, \gamma_i) = \frac{N(R_k, \gamma_i)}{N(\gamma_i)} \tag{3}$$

We normalize the distribution dividing it by the total:

$$n(R_k) \quad = \quad \frac{N(R_k)}{\sum_i N(R_i)} \tag{4}$$

4 Temporal Distribution

The considered questions are:

- What is the lightning frequency in the field of view of the sensor? What is the number of detected events and groups per frame and per second?
- How are the data correlated?

- What is the duration of flashes?

The LIS night-time data from the central pixels (± 50) were used for this first estimation. This avoids the bias from possible data reduction during the days due to low SNR. It can be expected that the short time characteristics of lightning are the same for day and night.

The observation time for any ground location is only about 90 s for LIS. This is between the time scales of flash duration and storm lifetime. Due to this sparse sampling a large number of orbits has to be taken for the analysis.

4.1 Number of groups per time interval

Groups per second The time series of number of detected groups per second is very sparsely filled with data. Only 0.57% of the seconds are non-empty, i.e. most of the time no lightning was detected. The mean number of groups per second is $0.118\,\mathrm{s}^{-1}$. If only the non-empty second intervals are considered a mean number of $20.7\,\mathrm{s}^{-1}$ is observed. Note that this holds for the matrix of 100×100 pixel (full is 128×128).

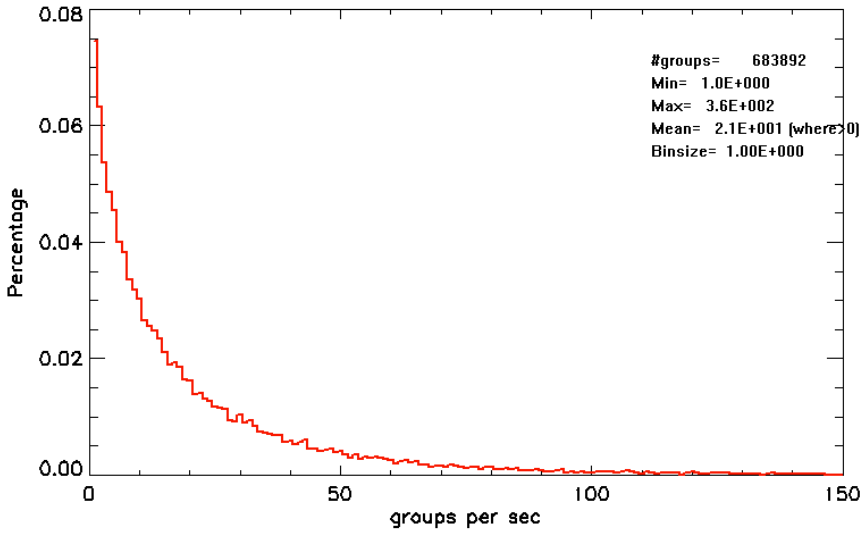

Figure 2: Number of groups per second. Normalized distribution. 90% of all 1 second intervals contain less than 50 groups.

Groups per 100 ms In order to investigate the sub second structure of lightning the distribution of groups in 100 ms intervals was calculated. As expected, this time series is even more sparsely filled than the 1 s time series. Only 0.2% of the intervals were non-empty. An overall mean of $0.118\,\mathrm{s}^{-1}$ is calculated. If only the non-empty 100 ms intervals are considered the mean number of groups increases to 5.5 $(100\,\mathrm{ms})^{-1}$

For the single 2 ms time frames we found that 87% contain only 1 group, 6% contain 2 groups.

This concentration of lightning at the small scales reflects the fractal structure of the lightning time series. The lightning frequency found here for the LIS data will be extrapolated to the geostationary field of view in section 9.2.

4.2 Autocorrelation

The autocorrelation function of the above time series is a measure for the persistence of lightning in time, i.e. the clustering of lightning into subsequent time intervals. This function was calculated for the 1 s- and the 100 ms-time series. Both functions show a very high concentration near the origin, the 1 s-function is almost delta-like (Figure 3). This is to be interpreted as the absence of long autocorrelation. The enhanced correlation between 2-80 s is caused by the lightning in a storm system during the observation time, which is limited to 90 s for any ground location.

The autocorrelation function for the 100 ms time series is concentrated in the first 0.8 s (Figure 4). This is consistent with the groups per 100 ms result: 80% of all non-empty 100 ms intervals contain less than 8 groups.

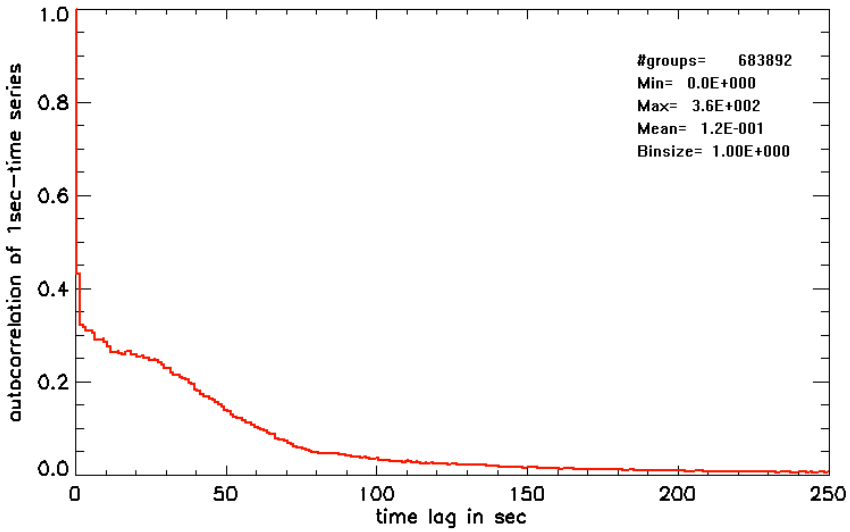

Figure 3: Autocorrelation function of the number of groups per second time series. The function is almost delta-like, i.e. there is a very low persistence.

4.3 Flash duration

The duration of flashes is calculated as the time difference between the last and the first group of a flash. For the analysed data 9% have minimal duration of less than 2 ms, i.e. consist of only 1 single group. The mean duration of flashes is 0.26 s and 0.30 s for multi-group flashes (longer 2 ms). The most frequent duration is 0.13 s. The histogram of the flash duration times (Figure 5) show a broad distribution within 1 s.

This result is in accordance with ground based lightning observation, were the majority of the multi-stroke lightning flashes have durations shorter 1 s.

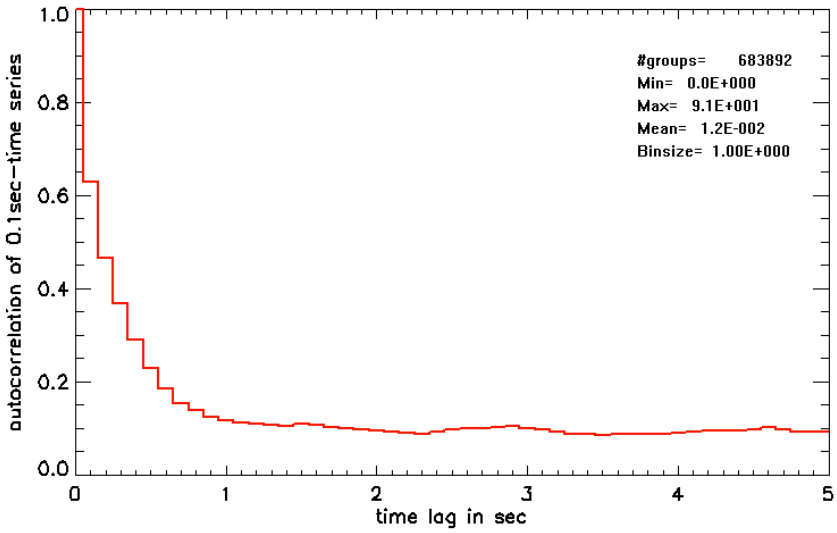

Figure 4: Autocorrelation function of the number of groups per 100 ms time series. The function drops to a constant low value during the first 0.8 s.

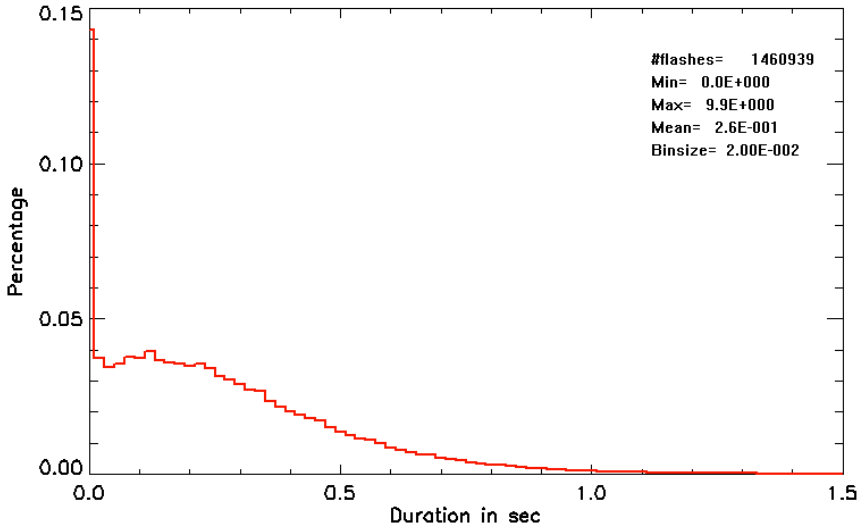

Figure 5: Duration of flashes. Normalised histogram with bin size 20 ms. 14% have duration shorter than 20 ms consist of only one group. The rest is mostly inside 1 sec

5 Spatial distribution

The considered questions are:

- What is the spatial size of lightning i.e. size of the groups?

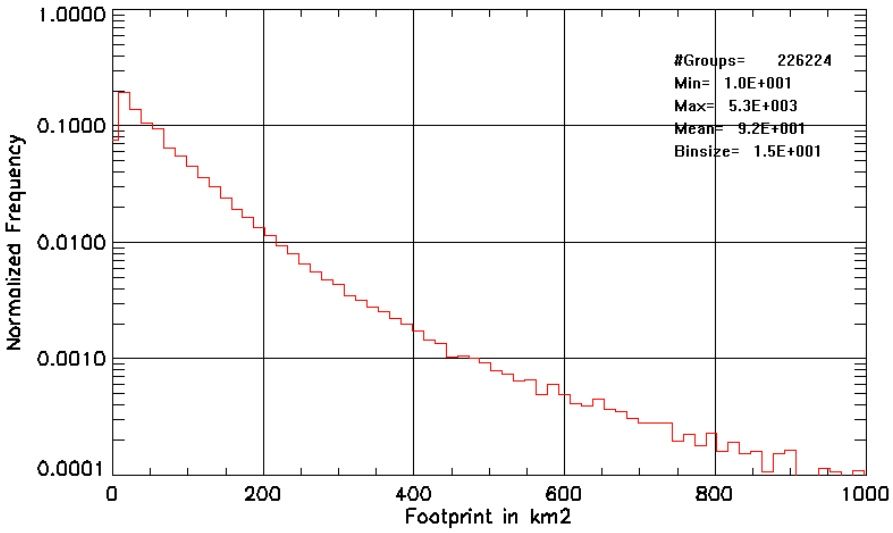

Figure 6: Footprint of groups, normalised histogram.

- How many pixels can be filled in one time frame of 2 ms?

As in the previous section LIS data detected only during night-time and from the central pixels (± 50) were used.

The ground footprint of the whole detection matrix is 550 km$\times$550 km. Hence the largest detectable lightning structure is limited by this value. It can be expected however, that most of the lightning fits within this size. This was verified by an additional examination of the OTD data which have a larger footprint.

The spatial resolution is determined by the pixel footprint, which is 3-6 km for LIS. Hence some of the small structure of lightning might be undetectable.

5.1 Footprint area of groups

The number of pixels belonging to one lightning group gives the estimate for the footprint of the whole group. The results show a minimum footprint of 10 km^2 for 20% of all groups corresponding to the pixel footprint. The number of groups then decreases almost exponentially for larger footprint areas. The mean footprint area is 92 km^2 and about 90% of all groups have footprint smaller than 200 km^2. If the shape of the groups is assumed to be circular (or square for small groups) the diameter of the groups can be calculated from the footprint area.

5.2 Number of events per 2 ms frame

In order to estimate the maximum number of pixels (events) which can occur in a single time frame of 2 ms all data for 2004 were analysed. In contrast to the above analyses all pixels and all times were used, the data were filtered only with respect to alert flags. The resulting distribution of number of events in the non-empty 2 ms is shown on Figure 7.

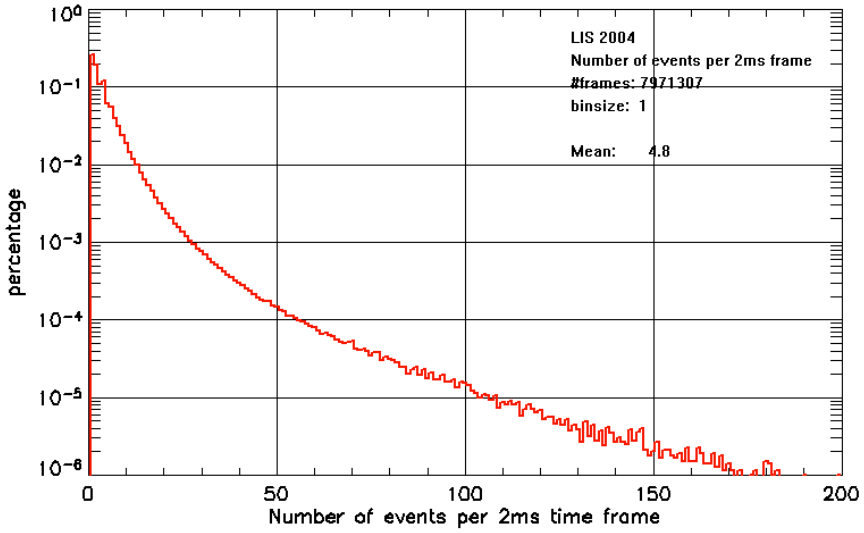

Figure 7: Number of events per 2 ms time frame.

We found that 90% of all frames have less than 10 events. The mean number of events per time frame is 4.8. The overall maximum was about 500 events (pixel) in one time frame, which is still a small number compared with the total number of 128^2 pixels, i.e. the pixel matrix is filled sparsely with lightning events at any time.
Most of the events in one time frame belong to the same group, i.e. are spatially close together. Thus, the above results will scale with the pixel resolution.

6 Lightning radiation

The lightning radiation is is the parameter with the largest uncertainty. The LIS instruments uses changing detection threshold in order to optimize the lightning detection during day in night conditions. Since we are interested in the characteristics of the *lightning source* only the night time data where the highest quality can be supposed were used in this section. The background radiation was minimal for these selected data. It is assumed that the radiation of lightning is the same for day and night thunderstorms.

The considered questions are:

- What is the radiance for lightning strokes (groups)?
- How is the radiance distributed in lightning flashes consisting of several groups?

The central pixel area used for the analysis was reduced to ($\pm$30) in order to avoid distortions in radiation determination in the off-boresight pixels (Boccippio et al., 2002).

6.1 Radiance of groups

The frequency distribution of the radiance of groups is shown on Figure 8. It exhibits a faster than exponential decrease toward the high radiation values. The minimum radiance is $\approx$3 μJ m^{-2} sr^{-1} due to

the sensitivity threshold of the pixels. Maximum group radiance was observed to 15,000 $\mu\mathrm{J\,m^{-2}\,sr^{-1}}$, but due to the upper detection limit of the sensor a saturation effect is noticeable at larger radiation values, i.e. largest amplitudes are mapped into lower bins. As written earlier, the radiance for events can vary between 3 $\mu\mathrm{J\,m^{-2}\,sr^{-1}}$ and 500 $\mu\mathrm{J\,m^{-2}\,sr^{-1}}$.

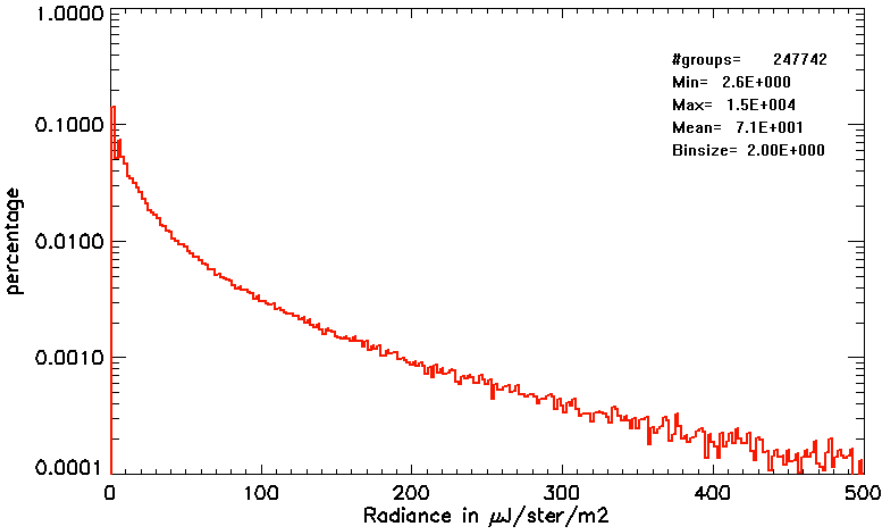

Figure 8: Radiance of groups, normalised histogram.

We note, that about 64% of all groups have a radiance above 10 $\mu\mathrm{J\,m^{-2}\,sr^{-1}}$.

6.2 Radiance per footprint area

We calculated the radiance per footprint area (Figure 9) which independent on the pixel size and resolution. It allows for the calculation of the energy which will be received by pixels with other than LIS footprint size.

Most frequent are values between 0.1-0.5 $\mu\mathrm{J\,m^{-2}\,sr^{-1}\,km^{-2}}$, but 42% of all data have radiances larger than 0.5 $\mu\mathrm{J\,m^{-2}\,sr^{-1}\,km^{-2}}$.

6.3 Maximum radiances in flashes

A lightning flash consists of several lightning return strokes, which are represented by the 'groups' in the LIS data set. A statistical analysis shows, that 65% of all flashes consist of more than 5 groups, with a mean number of 11.6 groups per flash. This corresponds to the broad distribution of flash duration found in section 4.3.

We calculated the distribution of the largest group radiance per flash (Figure 10).

For 90% of the flashes the brightest group has a radiance value >10 $\mu\mathrm{J\,m^{-2}\,sr^{-1}}$. This is of relevance for the detection efficiency. For many practical applications it is sufficient to detect the lightning flash but not necessarily each of its single groups.

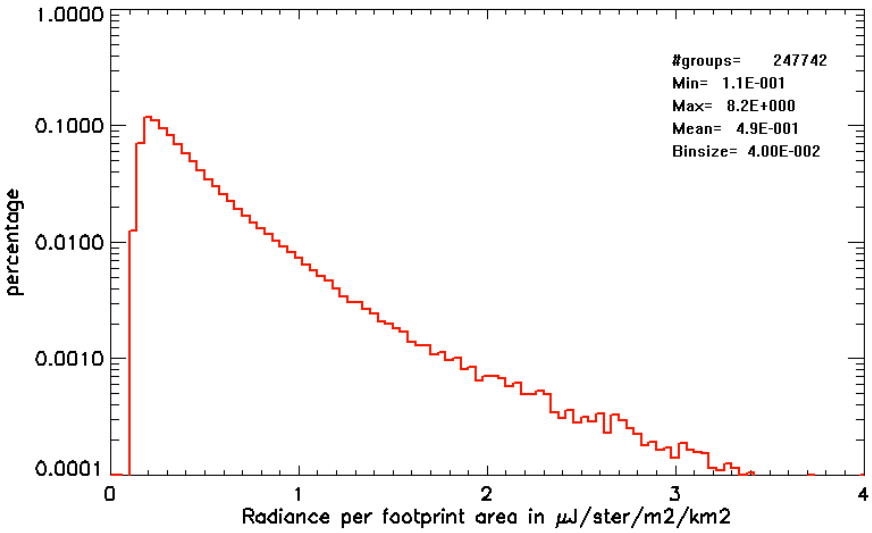

Figure 9: Radiance per footprint area of groups, normalised histogram.

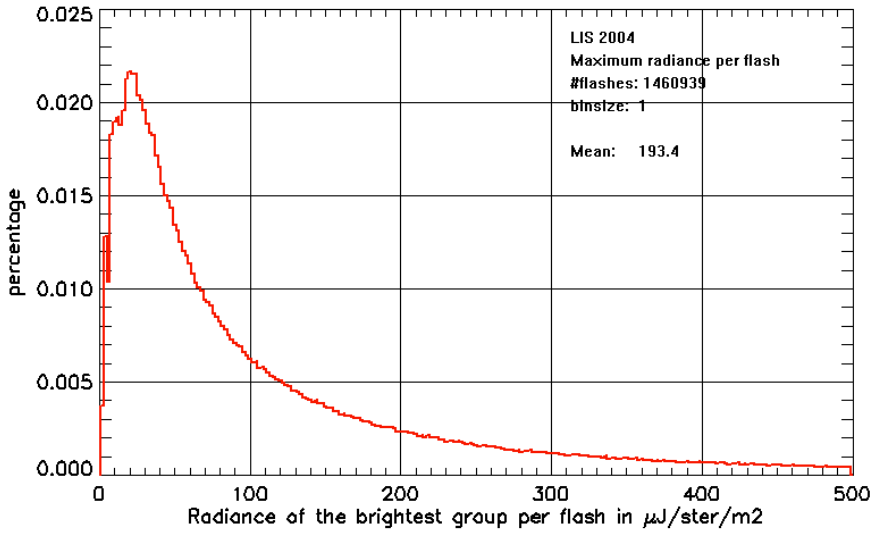

Figure 10: Distribution of the radiance of the brightest group in each flash. The most maximum radiances are in the range between 15-30 $\mu\mathrm{J\,m^{-2}\,sr^{-1}}$. Compare with the overall radiance distribution for the groups (Figure 8).

7 Random lightning generator

The results of the statistical analyses given in the previous sections can be used to simulate the signal from lightning as it appears on the top of the clouds. The simulated signal represents a random

distribution of lightning radiance. It can be utilized as input in instrumental studies.

In a first step the distribution of radiance and size of the lightning pattern are fitted to analytical functions. The second step generates random numbers according to these functions to simulate the random lightning radiance clouds.

7.1 Analytical distribution functions

The results of the statistical analyses of the previous section can be approximated by analytical distribution functions. The parameters of these distribution functions are determined by fitting to the empirical data.

Total Radiance R_0 The total radiance (see Sec. 6.1) is fitted by a Weibull-distribution

$$f(R_0) = \alpha\beta^{-\alpha} R_0^{1-\alpha} \exp\left[-(R_0/\beta)^{\alpha}\right] \tag{5}$$

with $\alpha = 0.55$ and $\beta = 30.0$ from the empirical statistical fitting.

Cloud size σ_0 The effective size of the lightning radiation cloud (see Sec. 5.1) is fitted by a Gamma distribution

$$g(\sigma_0) = \frac{\sigma_0^{\alpha-1} \mathrm{e}^{-\sigma_0/\theta}}{\Gamma(\alpha)\theta^{\alpha}} \tag{6}$$

with $\alpha = 0.225$ and $\theta = 3$ from the empirical statistical fitting.

The statistical analysis of the LIS data shows a high correlation between total radiance and size of the radiation pattern. A power law regression relation was found to

$$\sigma_0 = 0.6875 \cdot R_0^{0.323} \tag{7}$$

with correlation coefficient 0.94.

7.2 Simulation of lightning pattern

The radiance pattern of lightning can be simulated by a random lightning generator. For simplicity the lightning radiance cloud is assumed to be a circular Gaussian radiance cloud, i.e. has circular symmetry with a normal distributed radiance. The distribution of the radiance R at a location $\vec{r}$ in space is:

$$R(\vec{r}) = \frac{R_0}{2\pi\sigma_0^2} \exp\left[-\frac{(\vec{r} - \vec{r}_0)^2}{2\sigma_0^2}\right] \tag{8}$$

with the random variates $R_0, \vec{r}_0, \sigma_0$.

A set of N lightning clouds can be generated each with random position, random total radiance and size. The position of the centres are random according to the geographical distribution, for simplicity simply a uniform distribution can be assumed. Total radiance and spatial size of the clouds are generated as random numbers according to the distribution functions given in the previous section 7.1.

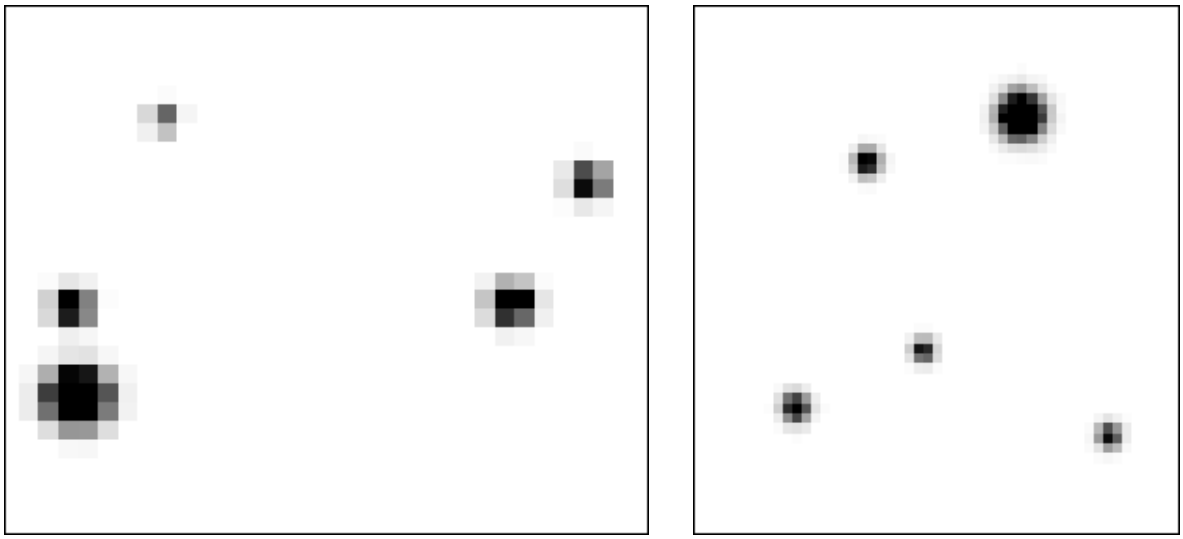

Figure 11: Simulated lightning radiance pattern detected by a pixel matrix with large pixel size (left) and smaller pixel size (right).

The temporal structure can be represented by generating the lightning clouds with time stamps, which are distributed according to the lightning frequency and the autocorrelation as found in the statistical analysis.

A random variate y which is exponentially distributed is generated from a uniform random variate u:

$$y = -\langle y \rangle \cdot \ln(u) \tag{9}$$

A random variate following a Weibull-distribution can be generated from an exponential distributed random variate y by:

$$R_0 = \beta y^{1/\alpha} \tag{10}$$

For each of the random sets $(R_0, \vec{r}_0, \sigma_0)$ a large number of photons is generated, which represent the radiance pattern. The photons are distributed normally around the centres and the total number of photons is proportional to the total radiance.

These randomly generated photon clouds can be used for studies of detection. For instance, in order to simulate the detection by a pixel matrix, the 2-dimensional histogram of the photon positions can be calculated with bin sizes representing the pixel size. An example is given in Figure 11.

The lightning generator is delivered as MATLAB® function in documented source code.

8 Background radiation

Lightning is aimed to be detected during night and day. Since the detection is in the visible wavelength range (777.4 nm) lightning has to be distinguished from the bright reflected solar radiation from the ground and cloud surfaces. The brightest background radiation originates from clouds, since the

albedo for land and water is normally lower than the cloud albedo. Exceptions are the high reflecting ice and snow surfaces and specular reflections from water.

The cloud surface is during the day illuminated by the sun. A large part of this solar insulation is reflected by the clouds according to their high albedo ranging between 0.5-0.9. This cloud illumination is the background on which the transient lightning flash signal has to be detected.

The radiance of the cloud surface depends on the solar zenith angle, on the cloud thickness and height. Also the cloud type, the cloud particle's phase and density are of importance. Particularly thunderstorm clouds with high cloud tops and high particle density can have the highest albedo values.

Maximum radiances are produced by specular reflections of the sun by water surfaces ('sun glint') which is observed for locations where the sun zenith angle and the satellite zenith angles are equal and sun, satellite and the viewed point are in a vertical plane. A sun glint angle θ_g, i.e. the angle to the specular reflection direction, can be calculated by:

$$\cos\theta_g = \cos\gamma_{sol}\cos\gamma_{sat} - \sin\gamma_{sol}\sin\gamma_{sat}\cos\phi \tag{11}$$

with γ_{sol} - solar zenith angle, γ_{sat} - satellite zenith angle, ϕ - relative azimuth angle between sun and satellite. For angles close to the glint angle the reflected radiation can be very large depending on the reflecting conditions on the water surface, i.e. the wave spectrum.

The relation between the lightning radiance and the background radiance determines the signal-to-noise ratio for the lightning detection and has strong impact to the detection quality parameters such as detection efficiency and false alarm rate.

The aim of this section is to characterize the cloud radiance in the considered wavelength interval 777.4 nm. The considered questions are:

- What is the background radiance distribution?
- What is the signal-to-noise ratio?

Data sources Information of the background radiation at the interesting wavelength was retrieved from the same satellite data set as the lightning data in the previous sections. Particularly the following data items were used:

1. The background images taken by the LIS which are available every 35 s. These data give an estimation of the radiance as seen by the detector in the 1 nm spectral interval around 777.4 nm.
2. The event's background radiance value. In the available lightning data for each event a background radiance value was associated, which was derived from the closest in time background image or from the solar zenith angle. These data give a conditionally sampled estimation for the background radiance for the areas were lightning occurred. Hence this allows for an a-posteriori determination of the signal-to-noise ratio.

Additionally the usability of the Meteosat visible images was examined as a further data source:

3. The radiance from geostationary cloud observation satellites (Meteosat) operating in the visible band. These data have a lower resolution in time, but can provide information about the distribution over the full visible disk.

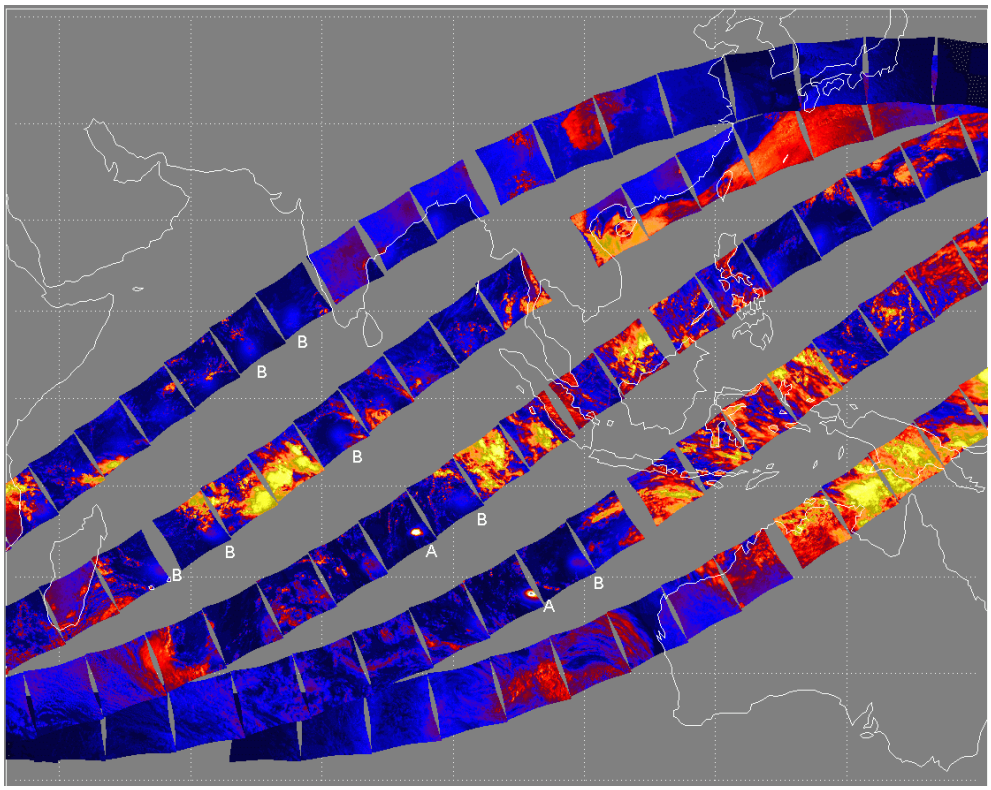

Figure 12: Geolocated images for the 9th Feb, 2004. For clarity only every 3rd background images per orbit is plotted. The letters (A,B) indicate sun glint: A strong glint, B weak sun glint.

8.1 Background Images

Background images are provided with the LIS data. They represent 128x128 pixel images which were taken in intervals of about 35 seconds. The dynamic range of the radiance in the images is 12 bit. The images were calibrated using the provided calibration files transforming thereby the data into the physical unit $\mathrm{W\,m^{-2}\,sr^{-1}\,\mu m^{-1}}$. The calibration is pixel wise using a calibration formula of 2nd degree polynomial:

$$R(i,k) = DC_0(i,k) + DC_1(i,k) \cdot B(i,k) + DC_2(i,k) \cdot B(i,k)^2 \tag{12}$$

The calibration files were compiled from the pre-flight laboratory calibration (Koshak et al., 2000).

Figure 12 shows the geolocated background images for 5 orbits across the Indian Ocean on the 9th Feb, 2004.

The LIS data for one year (2004) were used for the following analysis. During this year a total of about 5700 orbits are available with a yield of about 850,000 single background images.

It should be noticed that the geographical coverage is not uniform with latitude. At the highest latitudes (-35° and +35°), the turning latitudes, the observation time is larger. All the following statistics are therefore weighted by the effective viewing times.

The sun glint produces very high background radiances and can saturate the detector. Enhanced radiance due to sun glint can be seen in the data for glint angles <20° (see Fig. 12). The position of

the sun glint spot depends on the satellite position and the time. For a geostationary orbit the location of the sun glint pattern changes only with time.

8.1.1 Method of analysis

The complete data set for the year 2004 was processed. The sun glint was not eliminated from the data, since it is part of the variability of the background radiance signal. It was verified that the strong glint affects the results only in the highest radiances and can be easily identified.

As in the previous sections the outer pixels were not used and the analysis was confined to the central pixels ($\pm$50). Therefore a correction of the larger pixel footprint for the offboresight pixels (Boccippio et al. (2002)) was not necessary here.

The frequency distribution of the radiance values were calculated. All results were weighted by the viewtimes. The distributions are normalized to their totals.

8.1.2 Total radiance distribution

A total number of 856218 image frames was processed. The background radiance varies between 0 and 600 $\mathrm{W\,m^{-2}\,sr^{-1}\,\mu m^{-1}}$. The lower most radiance values ($\leq 5\,\mathrm{W\,m^{-2}\,sr^{-1}\,\mu m^{-1}}$) are observed in the night frames.
The mean and standard deviation values for day and night are:

radiance (in $\mathrm{W\,m^{-2}\,sr^{-1}\,\mu m^{-1}}$)	day	night
mean value	158	0.1
standard deviation	155	1.0

The normalized radiance distribution function for all data is shown on Figure 13. Between 50 and 400 $\mathrm{W\,m^{-2}\,sr^{-1}\,\mu m^{-1}}$ the radiance distribution function decreases almost exponentially. These values originate from reflected solar radiation by land and sea surfaces and clouds. Radiances larger than 400 $\mathrm{W\,m^{-2}\,sr^{-1}\,\mu m^{-1}}$ correspond to high bright clouds. The secondary maximum between 500-600 $\mathrm{W\,m^{-2}\,sr^{-1}\,\mu m^{-1}}$ is caused by sun glint over water surfaces.

The following table shows the frequency of images with radiances larger than a certain threshold:

Threshold radiance ($\mathrm{W\,m^{-2}\,sr^{-1}\,\mu m^{-1}}$)	300	400	500
Frames with radiances above threshold	132777	31767	3148
Percentage of all daytime frames	30%	7%	0.7%

8.1.3 Variation with solar zenith angle

The reflected radiation from clouds strongly depends on the solar zenith angle (SZA). Assuming the reflecting surfaces to be Lambertian, the reflected radiance scales with the cosine of the SZA: $R(\gamma_{sol}) \sim I_0 \cos\gamma_{sol}$, for $\gamma_{sol} < 90°$. To analyse this dependency all pixels were associated to the SZA of the boresight location (i.e. of the central pixel) of the corresponding image.

Figure 14 shows the resulting 2-dimensional frequency distribution of radiance values with the SZA. For SZA >95°, i.e. during local night time the detected radiances were $\leq$5 $\mathrm{W\,m^{-2}\,sr^{-1}\,\mu m^{-1}}$. For twilight conditions (85°$<$ sza $<$ 95°) radiances reach up to 100 $\mathrm{W\,m^{-2}\,sr^{-1}\,\mu m^{-1}}$.

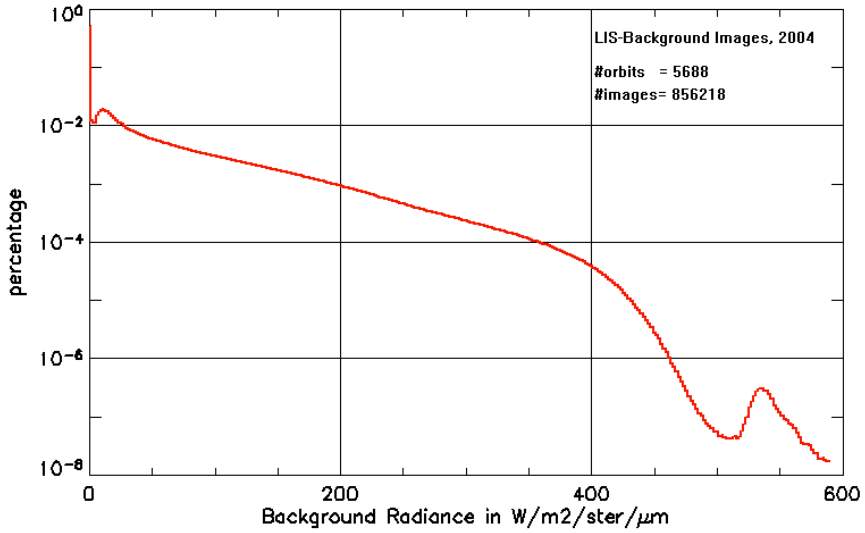

Figure 13: Frequency distribution of background radiances.

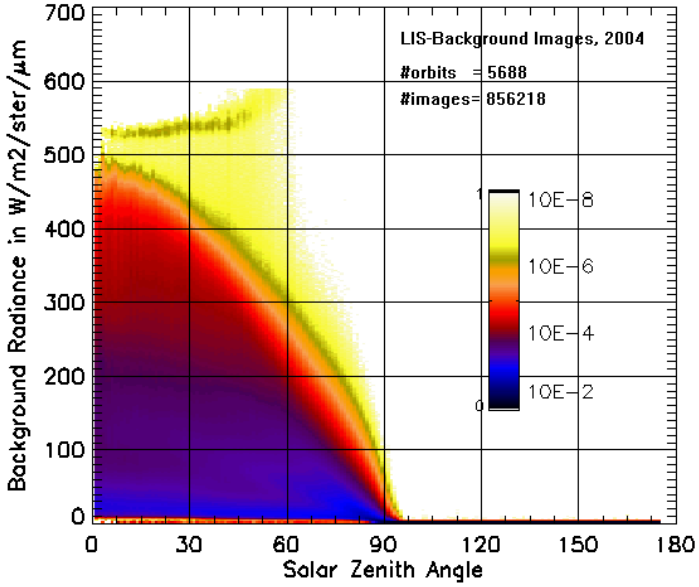

Figure 14: Frequency distribution of background radiance as function of SZA. Note the appearance of sun glint for radiances above 500 $\mathrm{W\,m^{-2}\,sr^{-1}\,\mu m^{-1}}$.

	day (sza<90°)	night (sza≥90°)	total
number of images	432853	423365	856218
percentage	51%	49%	

Figure 15 shows the radiance distribution separately for day (sza<90°) and night (sza≥90°).

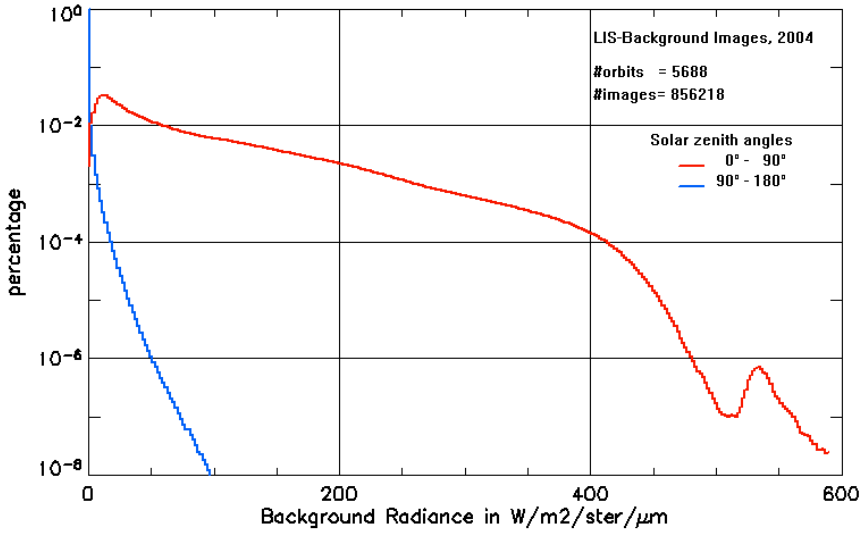

Figure 15: Frequency distribution of background radiance for day-time (sza$<$90°) and night-time (sza$\geq$90°). Both curves are normalized

During the local daytime the largest radiances values occur at the lowest SZA.

For a geostationary orbit the SZA distribution in the field of view depends only on UTC. Hence the dependency on the SZA found here can be used to parametrize the radiance distribution for a geostationary observation (see Sec. 9).

8.1.4 Other dependencies

The distribution of the reflected radiance from ground and from clouds depends on a variety of other meteorological and geographical parameters. This includes land-sea, latitudinal and seasonal variations and the variation with the local solar time. The cloud type and occurrence depends on the atmospheric conditions such as moisture content, stability and others. All these variations depend on specific locations and on many time scales and will not be considered in this statistical analysis. We suppose, that the main characteristics of the background radiance with its statistical variability is sufficiently described by the SZA-dependence.

8.2 Event background radiance

The LIS lightning data contain for each event a value of the corresponding background radiance. This value is estimated from the closest in time background image or from the SZA. These background radiance data represent a conditionally sampling with respect to the detected lightning events. Background radiance of cloud free areas and non-convective clouds are not contained in these data.

The data were filtered as previously (Sec. 3.1) in order to remove data with alert flags and data from the non-central pixels.

8.2.1 Total frequency distribution

Figure 16 shows the distribution of the background radiance corresponding to the detected lightning events. It is nearly uniformly distributed in the range 10-400 $\mathrm{W\,m^{-2}\,sr^{-1}\,\mu m^{-1}}$. High background

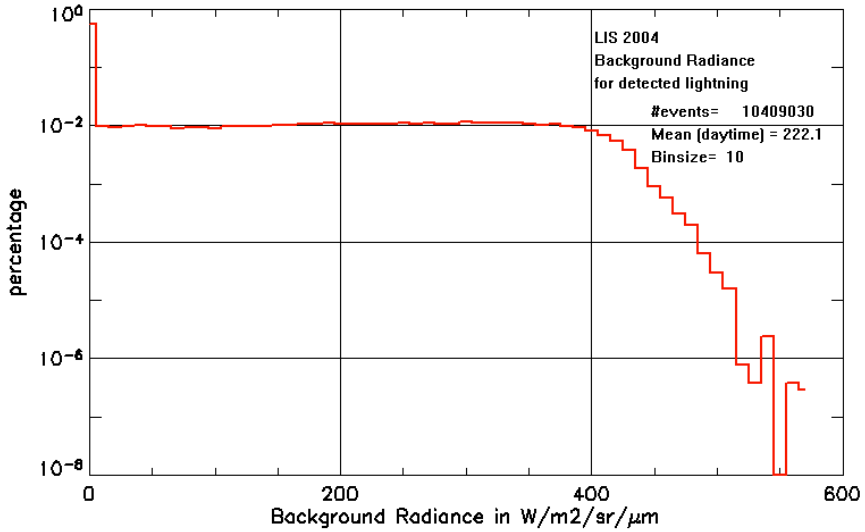

Figure 16: Background radiance distribution for the detected events. High background radiances are more frequent than in Fig. 15 since storm clouds are usually bright reflecting clouds.

radiances are more frequently in this sub sample than in the total data (cf. Fig. 15). The reason is the higher albedo of thunderstorm clouds due to their high optical thickness. The mean background radiance for daytime (SZA<90°) is 222.1 $\mathrm{W\,m^{-2}\,sr^{-1}\,\mu m^{-1}}$. The peak at smallest radiances originates from the night-time data.

8.2.2 Variation with local solar time

The thunderstorm occurrence exhibits an expressed diurnal cycle which is closely connected to the solar insulation. Due to the meteorological mechanism of storm generation the storm as well as the lightning activity peak in the local afternoon hours and decrease slowly during the night. Since the event background data are conditionally sampled for the lightning events a pronounced variation with the local solar time (LST) can be expected. This is confirmed by the results of the statistical analysis.

Figure 17 shows the distribution of background radiance with the LST. During the daytime hours, the mean background radiance increases primarily due to the decreasing of the SZA (see next section). Since storms are more frequent in the afternoon hours, the corresponding bins in the histogram are higher populated.
During the night (19-5 LST) the background radiation is very low.

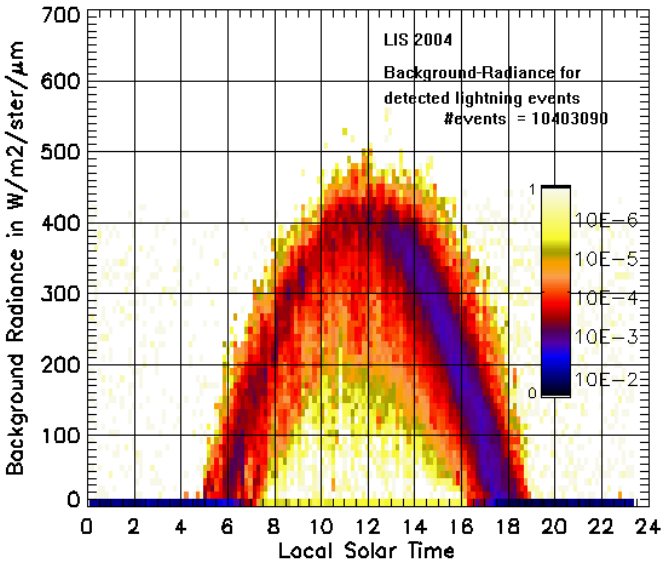

Figure 17: Background radiation for detected events as function of local time. The logarithmic colour scale indicates the frequency of observation of a certain radiance and LST. Note the higher number of events in the afternoon hours which reflects the well-known diurnal cycle of thunderstorm activity. The function is viewtime corrected and normalized.

8.2.3 Variation with solar zenith angle

As found in section 8.1.3 the background radiance depends strongly on the SZA. This is confirmed here for the event background radiances (Fig. 18).

Compared with Figure 14 the distribution is now concentrated in the higher radiances since lightning appears more frequently in the brightest clouds for a given SZA. Note that the sun glint radiances do not appear in this result, since these data are marked with the glint alert flag and were filtered out.

The empirical function can be fitted by a function expressing the combined frequency distribution of radiance and SZA:

$$f(R,\gamma_s) = (2\pi S_m)^{-1} \cdot \exp\left[-\frac{(R - R_m \cdot \cos(\gamma_s))^2}{2S_m^2}\right] \tag{13}$$

i.e. a normal distribution with the empirical found parameters $R_m = 390\,\mathrm{W\,m^{-2}\,sr^{-1}\,\mu m^{-1}}$ and $S_m = 34\,\mathrm{W\,m^{-2}\,sr^{-1}\,\mu m^{-1}}$.

8.3 Meteosat visible images

The visible channel of the geostationary satellite Meteosat-7 detects radiation in the 0.45-1.0 μm band. This includes the 0.7774 μm wavelength used for lightning detection. The analysis of the Meteosat images thus opens the possibility to analyse the background radiance from the entire visible disk.

Various climatologies of the visible radiation data exists in the literature.Here we will present only a single statistical distribution in order to demonstrate the potential benefit of these data. The visible

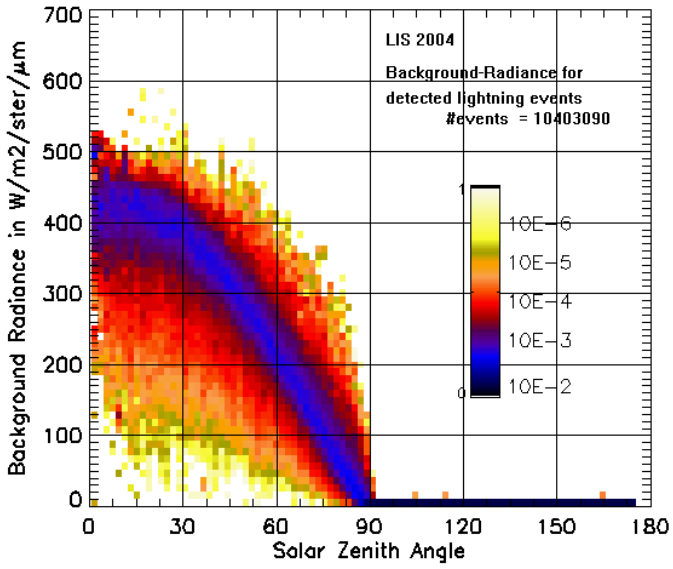

Figure 18: Frequency distribution of background radiance and SZA for the detected events. The colour indicates the frequency of observation of a certain radiance for a SZA. The function is weighted with SZA frequency and normalized.

images for the year 2004 were used. Data were available between 0530-1900UT with 30 minute repetition rate. The resolution was reduced from the original to 2500×2500 pixels, this corresponds to a spatial resolution of 5 km×5 km at nadir. The data were used in the 8 Bit counts gray values as provided from EUMETSAT.

The frequency distribution of the radiance values per pixel was calculated. The result is shown in Figure 19. The curve shows a similar shape as the background radiance distribution detected with the LIS. Since LIS and Meteosat have different spectral response curves a direct comparison will not be discussed here. The used data were limited to the 0..255 counts (1 Byte range), hence, a saturation in the upper radiances bins due to sun glint is evident.

Maximum radiances The largest radiances originate from bright clouds, but also from solar glint and reflections from ice and snow surfaces. To visualize the statistical distribution of the largest radiances the frequency of pixels exceeding a radiance threshold of 150 counts (corresponding to $\approx$120 $\mathrm{W/m^2/sr}$) was calculated for the entire year 2004. The result (Fig. 20) shows a high frequency of bright radiances for the inner tropical convergence zone (ITZ) where high convective clouds with large albedo and low SZA yield large values of reflected solar radiation. Large radiance values are also observed for large satellite zenith angles γ_{sat}, i.e. in the outer ring of the visible disk. The cloud areas contributing to these pixels scale with $1/\cos\gamma_{sat}$, thus the detected radiance can get very high, particularly for high reflecting surfaces such as ice and snow in the polar and sub polar regions.

The above brief analysis shows that the Meteosat visible images can be a valuable data source for estimating of the background radiances during the course of the day. If the solar reflection can be assumed to be constant with frequency in the 0.45-1.0 μm band, then using the spectral response function of the Meteosat radiometer the radiance at the wavelength 777.4 nm proposed for lightning

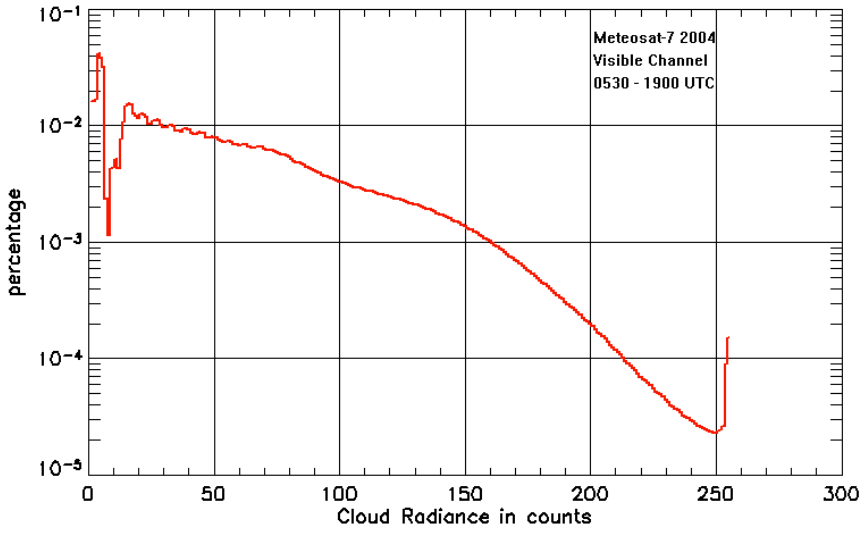

Figure 19: Meteosat visible channel. Distribution of the radiances for 2004 in counts of gray values. The maximum radiance are due to saturation from sun glint and very low slanting angles

detection can be estimated.

8.4 Signal-to-Noise ratio

For the detected lightning the ratio between the radiances of lightning and the background illumination was analysed. This gives an estimation for the signal to noise ratio (SNR).
The radiation data for lightning and background are stored in the data in different units. The transient radiation from lightning is given in $\mu\mathrm{J\,m^{-2}\,sr^{-1}}$ as the energy E_{LI} which was gained by the detecting pixel. In contrast, the slowly changing background radiance is stored as a radiance in units of $\mathrm{W\,m^{-2}\,sr^{-1}\,\mu m^{-1}}$. For the calculation of the SNR the background data I_{BG} were transformed into energy values E_{BG}:

$$E_{BG} = I_{BG} \cdot \Delta t \cdot \Delta\lambda \tag{14}$$

with the frame integration time $\Delta t = 1.9 \cdot 10^{-3}\,\mathrm{s}$ and the width of the wavelength filter $\Delta\lambda = 0.909 \cdot 10^{-3}\,\mu\mathrm{m}$. This yields E_{BG} in the energy units $\mu\mathrm{J\,m^{-2}\,sr^{-1}}$.

We define the SNR as the ratio of the lightning radiance to the sum of lightning and background radiance:

$$\mathrm{SNR} = \frac{E_{LI}}{E_{LI} + E_{BG}} \tag{15}$$

This SNR was calculated for all the LIS lightning events for the year 2004. For this analysis the data for *groups* were used instead of *events*. By this means, the radiance of a lightning channel was not split between the detecting pixels. The result is shown on Figure 21.

The SNR shows different behaviour for day and night conditions. During the day with bright background the SNR is lower than 0.5. The lowest SNR is even the most frequent during the day. This finding demonstrates the effective working of the on-board real time event processing (RTEP), which is able to distinguish the weak transient lightning signal from the bright background.

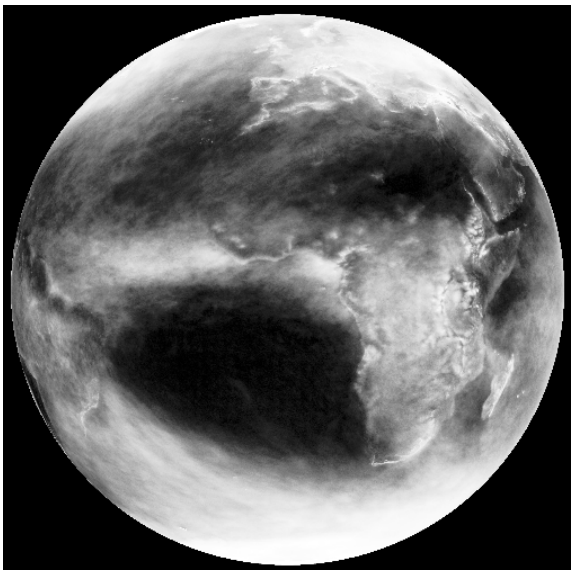

Figure 20: Meteosat visible channel. Frequency of radiances above $120\,\mathrm{W/m^2/sr}$ for 2004. The image was histogram equalized for contrast enhancement. The inner tropical convergence zone covered frequently with high clouds is distinguished as well as the outer ring areas of the visible disk particularly at the higher latitudes.

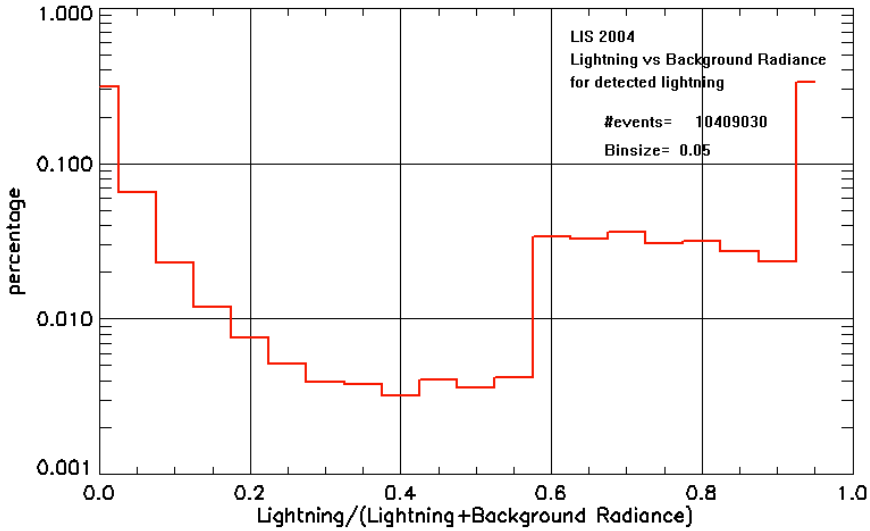

Figure 21: Frequency distribution of the signal to signal+noise ratio, SNR (for the definition see the text). SNR>0.5 is generally observed during the night times, while for the day time conditions the SNR<0.5.

During the night the SNR is >0.5. Background radiance is very low (see Sec. 8.1.3), these low discrete values cause the step-like behaviour of the distribution function close to 1. The high population

in the highest bin > 0.9 is due to background radiance equal to zero.

8.4.1 How to detect lightning on the background?

Background radiance is large during daytime and exhibits large variations. The maximum bg-radiance depends strongly on SZA (roughly with $\cos \gamma_{sol}$). Even on the same frame the background radiance can span over the range of 2 orders of magnitude. The lightning flash signal is on top of this bright background. Its radiance and energy collected during the integration time is mostly lower as shown in the previous section, also in the spectral window 777.4 nm. Consequently, lightning is recognized not by its bright radiance, but rather by its transient short pulse character. Thus for lightning detection a variable threshold has to be used for each pixel which takes into account for the changing background radiance.

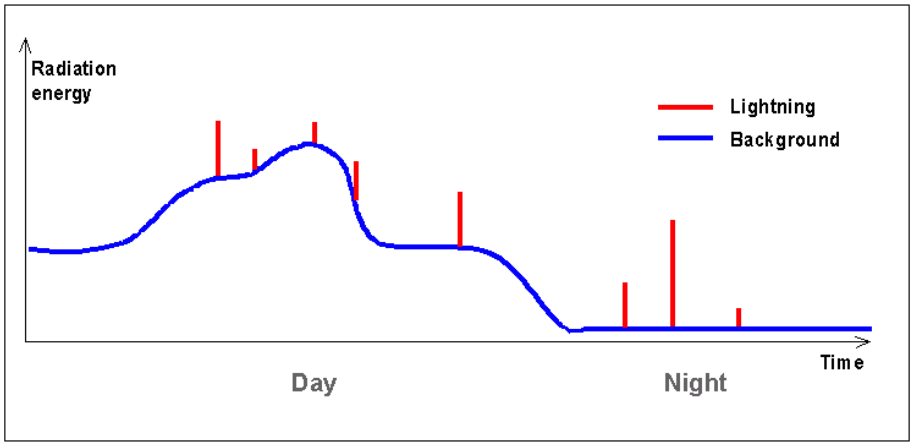

Figure 22: Scheme of lightning and background signal changing with time. Lightning is very short (< 2 ms) but weak in amplitude.

NASA has implemented in the lightning detection instruments OTD and LIS an on-board real time event processing (RETP) algorithm (Christian et al., 1995, 2003). This algorithm detects differences between the subsequent 2 ms frames and a background radiance, which is calculated as a moving average. Hence the pixel detection is performed on board, only the lightning information is transmitted to ground. This is a drastic data reduction while the high sampling rate of 2 ms is conserved.

9 Transformation to geostationary orbit

The results of the previous sections for the distributions of temporal, spatial and radiation characteristics of lightning and the background are generalized to the geostationary orbit (GEO).

9.1 Changes in observation geometry from LIS to GEO

Due to the 100 fold higher altitude above ground the geometry of observation is changed significantly.

parameter	LIS	GEO
altitude above ground	350 km	35,800 km
viewing angle from satellite	80°	17.4°
IFOV on Earth	5.4°	162.4°
IFOV on Earth (km)	550 km×550 km	full disk
viewing angle of 10 km distance at nadir	1.6°	0.016°
highest satellite zenith angle	42.7°	90°

Table 3: Geometrical parameters of the LIS and the geostationary orbit

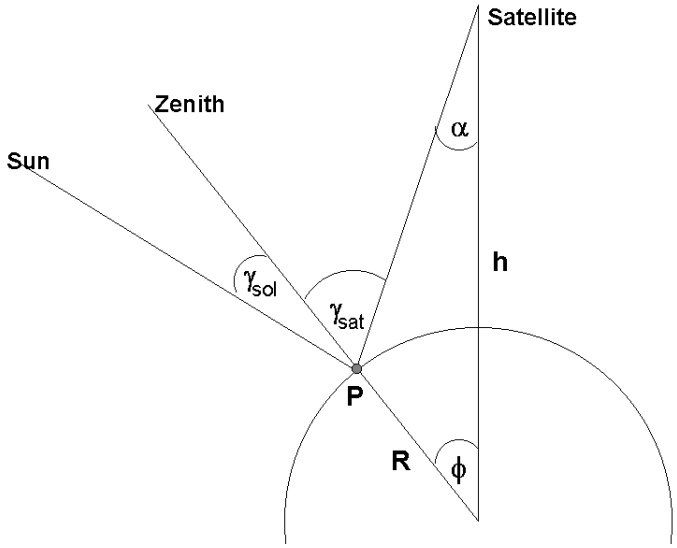

Figure 23: Satellite viewing geometry

The instantaneous field of view is the full disk and constant with time. The satellite zenith angle γ_{sat} can reach high values up to 90°. It is calculated for the ground location at longitude λ and latitude ψ by

$$\tan \gamma_{sat} = \frac{\sin \phi}{\cos \phi - R/(R+h)} \tag{16}$$

with ϕ the angle between nadir point of GEO (0,0) and the (λ, ψ) location on Earth:

$$\cos \phi = \cos \psi \cos \lambda \tag{17}$$

Since the footprint of the pixels scale with $1/\cos \gamma_{sat}$ it can be very large for the outer regions of the disk. Hence all the pixel based information needs to be related to a larger footprint.

9.2 Extrapolation of LIS results to GEO

9.2.1 Temporal distribution

The mean frequency of detected groups ($0.118\,s^{-1}$) which was found in section 4 is extrapolated to the full disk. The sampling area of the LIS instrument is 550 km × 550 km on the ground. Since only the central 100 of 128 pixels were used this reduces to $2.4\,10^5$ km^2. LIS is confined to the $\pm 35^\circ$ belt where most of the lightning occurs. A GEO sensor would see ≈1/4 of this 35° belt corresponding to an area of $7.8\,10^7$ km^2. From the ratio of both areas (appr. 330) a number of 40 groups per second is to be expected for the GEO-FOV.

As published by Christian et al. (2003) the mean global *lightning flash* rate amounts $47\,s^{-1}$. The contribution from Africa and Europe is about 1/3. Hence a *lightning flash* rate of $16\,s^{-1}$ can be expected for the GEO-FOV. The diurnal variation is about 30%. A flash consists of several single lightning strokes alias 'groups' in this work. Hence, the rough estimate of a number of 40 groups per second is in good agreement with this lightning flash frequency value.

9.2.2 Spatial distribution

Due to the larger IFOV more lightning events will be detected at the same time. Applying the same extrapolation as for the lightning rate and assuming a nadir pixel footprint of 6 km×6 km, we estimate a mean number of ∼300 responding pixel for the non-empty 2 ms - frames.

An important difference to the observation from low orbit is that the pixels are fixed to their footprint on Earth. Thus any inhomogeneity in pixel detection efficiency has a permanent impact on the corresponding geographic area. In case of a pixel failure the corresponding geographical area will get no lightning information.

9.2.3 Radiance of lightning

The radiance data of the lightning events are independent on the field of view. However, the increasing footprint with higher satellite zenith angle, can simply lead to higher radiance values at these pixels.

Furthermore, for higher satellite zenith angle the side walls of the clouds are observed as well. For special cloud configurations the lightning detection can be hampered. For instance, in case of an anvil cloud which can obscure the lightning in the clouds below. On the other hand, lightning from lower cloud levels might be detected with higher radiance through the side walls for tall convective cloud towers.

9.2.4 Background radiance

The background radiance $R(\lambda, \psi, t)$ for any location and time scales with the satellite viewing angle (γ_{sat}) the SZA (γ_{sol}) which is a function of time:

$$R(\lambda, \psi, t) \sim I_0 \frac{\cos(\gamma_{sol}(\lambda, \psi, t))}{\cos(\gamma_{sat}(\lambda, \psi))} \tag{18}$$

This dependence can lead to enhanced radiance in the outer part of the observed disk, as seen e.g. on Figure 20 for the Meteosat visible channel.

9.2.5 Other features

Solar glint position is a function of time only. The daily track of the sun glint changes slowly with the sun's declination. Therefore, unfavourable conditions may persist for longer time at the corresponding ground locations.

Since the sun glint occurs in the cloud free areas, these extraordinary high radiances will not directly affect the lightning detection in clouds. However, in broken cloud fields and at large satellite zenith angles the parallax effect can cause glint spots very close to real lightning. Hence, false alarms can be produced depending on the flash detection algorithm.

Direct solar signal may fall in the detector. To prevent this the FOV should be baffled to a smaller disk.

10 Scattering simulation

The previous sections presented a statistical analysis of the lightning observation data from the LIS instrument. The data represent the optical signal which was radiated from the upper surface of the cloud as a result of the multiple scattered radiation which was originally emitted by lightning. In this section a computer model is developed and applied for the simulation of radiation transfer from the lightning source up to the upper cloud surface. This gives the possibility to study the impact of the various parameters of the lighting source and the cloud on the observable radiation field. The simulation model strongly simplifies the real scattering process, but nevertheless the comparison of the results show a good agreement with observations.

10.1 Radiation transfer in clouds

Radiation transfer in the atmosphere and in clouds is a complicated process and depends on atmospheric conditions and a large number microphysical characteristics of the clouds.

There is a long lasting research and developing of methods for the calculating and modelling of the radiation transfer. Beside the numerical solution of the radiation transfer equations various Computer simulation methods were developed, the most prominent being Monte-Carlo simulation or ray tracing techniques. Less experience exists in the treatment of the transport of lightning radiation through clouds. Earlier studies were published by Thomason and Krider (1982) and Koshak et al. (1994). Recently, with the advent of the lightning detection from satellites these studies were continued and applied to the detected optical signals particular from the FORTE satellite (Light et al., 2001) but also for the lightning observation on Jupiter by the Galileo space probe (Dyudina et al., 2002).

Light is scattered in clouds by the interaction of the light wave with the cloud particles. In the case of spherical water particles (cloud drops) a good approximation is given by the Mie-theory. The presence of ice particles and drops of non-spheric shape complicate the description significantly. Elaborated theories and methods exist for quantitative description of the radiation transfer in the atmosphere and in the clouds in various conditions.

The aim of the scattering simulation which was developed as part of this study is to give a simple and easy to use method for the calculation of the radiation pattern which is produced by lightning on the

top surface of the clouds. It gives a possibility to demonstrate the influence of the various cloud and lightning parameters on the radiation distribution on the clouds surface and which can be detected by a satellite based sensor.

We assume that the complete scattering process on the cloud particles of different shape, size and phase can be represented by an effective scattering function which corresponds to a isotropic diffusion radiation transfer. The model is therefore strongly simplified and idealized. The justification for this idealization is the relative insensitivity of the multiple scattering in optically thick clouds to the microphysical characteristics (particle shape, phase and size distribution and number distribution). The driving bulk parameters considered here are the optical depth, the mean free path length and the cloud size. It must be admitted that even these parameters are largely unknown for the actual situation. On the other hand this simplification will limit the interpretation of the results on a more general level and adds a larger uncertainty to the calculated quantities.

10.2 Simplified scattering model

We give a short description of the model and its parameters. A more detailed and mathematical formulation is given in appendix A.

We assume Mie-scattering in the Henyey-Greenstein-approximation which is given by the following phase function:

$$p(\cos\theta) = \frac{1-g^2}{(1+g^2-2g\cos\theta)^{3/2}} \tag{19}$$

with $g = \langle\cos\theta\rangle$ - the asymmetry parameter being the mean cosine of the scattering angle. For visible and near infrared radiation scattering in clouds of water droplets the asymmetry parameter g varies between 0.81-0.88 (Light et al. (2001)).

A photon moves straight a path free of interactions between the scattering events. Scattering is elastic, it means deflection of the photon from the old direction to a new one (Figure 24).

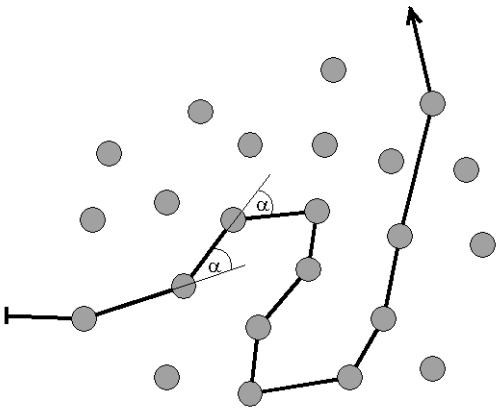

Figure 24: Multiple scattering process. The anisotropy of scattering is lost after multiple scattering events.

After multiple scattering processes the directional information is lost and the multiple scattering process can be approximated by an isotropic diffusion process (Light et al., 2001; Davis and Marshak, 2002). The free path length is substituted by an effective free path length $\lambda_e = \lambda_g/(1-g)$.

The described scattering process is realized as a random walk process in 3 dimensions with random free path lengths between the scattering events. These random path lengths follow an exponential distribution with a density function

$$f(\lambda_e) = \frac{\exp^{-\lambda_e/\alpha}}{\alpha} \tag{20}$$

where $\alpha = \langle \lambda_e \rangle$ is the mean free path length. This random walk is realized for a large number of starting photons with a Monte-Carlo model. The output is a set of stochastic variables describing the result of the scattering. The used parameters are described in the next section.

We will not consider absorption in our model though it can be easily introduced (Prahl et al., 1989, see e.g.). Instead, we ignore photons which did not come out of the cloud after a large number of scattering events. The used model is too crude, the uncertainties will mask the small effects from an improved absorption parametrization.

10.3 Parameters of the model

10.3.1 Input parameters

The following set of parameters are to be defined:

- scattering process parameters,
- geometrical sizes of the cloud,
- the lightning source geometry and emission strength, and finally
- the position of the lightning channel with respect to the cloud.

Scattering parameters The scatter parameters are the optical depth τ and the asymmetry parameter g. For the following simulations isotropic scattering, i.e diffusion approximation was used. In this approximation the specific optical depth is expressed by its inverse, the rescaled free path length λ_e. The use of the isotropic diffusion approximation uses much computation time. We believe that the approximation is well satisfied for optically thick clouds. Deviations will occur close to the cloud boundary. This is acceptable in view of the other uncertainties of the method. However the model is able to handle $g > 0$ as well.

More advanced phase functions can be introduced in order to describe the cloud composition more precisely.

Cloud geometry We assume the shape of the cloud as a plane parallel plate (e.g. 60km horizontal size and 14km vertical size.)

Light et al. (2001) used various idealized cloud shapes: cubical, spherical, cylindrical and horizontal plate clouds. They found differences between these cloud types particularly for the fraction of photons escaping through the side walls of the clouds.

If the cloud is large, optically thick and the scattered lightning radiation occupies only a small part of the cloud, then the driving parameter is the distance between the source and the outer cloud surface. This distance determines the spread of the radiation distribution pattern on the cloud surface. This assumption seems to be quite realistic, since thunderstorm clouds have horizontal sizes of at least few 10km, while the most lightning channel length are shorter than a few km.

Hence we focused on the analysis of the scattered pattern for the case of parallel cloud plate. The results can be easily transformed to other orientations of cloud surfaces. Hence for simulation and different satellite viewing angles only the orientation of the cloud surfaces to the satellite is important together with the distance of lightning from the outer surface.

Lightning source geometry and temporal characteristic It is well know that lightning has a branching fractal structure which is hard to describe satisfactory by an analytic function. On the other hand most of the details of the geometrical structure will be lost and smoothed during the scattering process. The used approach in the model is to input the lightning channel as a set of point sources which can be aligned and oriented in any way. Lightning channel lengths between 1 and 7 km are realistic though larger channels are observed as well.

The emission strength, i.e. the number of photons originating from each of the source points can be set arbitrarily. This is a free parameter in the model, which can serve to adapt the output to observed radiance values.

Each source location point ($\vec{r}_0$) emits a number of photons according to the emission strength (e_0). The initial direction of the photons (θ_0, ϕ_0) is assumed to be completely isotropic. The result of the scattering process is a photon distribution on the upper and the lower surface of the cloud. For extended lightning channels the resulting distribution can be simply calculated by the superposition of the results for the points constituting the line source.

The temporal characteristic of the lightning source was assumed to be a delta-like momentary release. In more elaborated versions a source varying with time can be implemented.

Lightning position with respect to the cloud The position of the lightning source within the cloud determines the time and the distance the photon has to travel by multiple scattering until it reaches a cloud surface. Hence, the key parameter in our model is the vertical distance to the nearest surface. Typically for diffusion a spreading proportional to the square root of the distance is expected.

Lightning can also appear outside of the cloud, as in the case of the lightning return strokes to the ground. This case differs from the intracloud lightning sources. The photons now will travel first straight without deflection until the rays enter the cloud crossing the lower cloud surface, where the scattering starts. Hence there is an 'geometrical' isotropic spherical wave spreading below the cloud. Obviously only the photons with initial upward direction angles will reach the cloud. The ground is assumed to perfectly absorbing.

10.3.2 Output variables

Output variables are the single photon parameters on exit and the calculated average and distribution functions for the ensemble of photons. From these distribution functions the interesting 'observables' can be derived.

When the photon reaches the surface of the cloud it preserves its actual direction, no farther scattering. The exit position (x, y, z) and the direction angles (ϕ, θ) with respect to the cloud coordinate system of each photon is stored. For further analysis the photons are classified with respect to their exit surface in upper and lower photons. Additionally the number of scattering events N and the total length of the path inside the cloud δl are saved. From this total path length the time delay δt of the photon is calculated.

The contributions from each of the photons i are summarized and binned yielding frequency distribution functions for the above listed quantities. These quantities can then be transformed for the field of view of a satellite.

10.4 Point source and superposition

10.4.1 Results for a point source

The model was tested for the elementary single point source at the various positions in and below the cloud.

$$I_0(x, y, z) = I_0\, \delta(x - x_0)\delta(y - y_0)\delta(z - z_0) \tag{21}$$

The resulting radiation pattern is shown on Figure 25

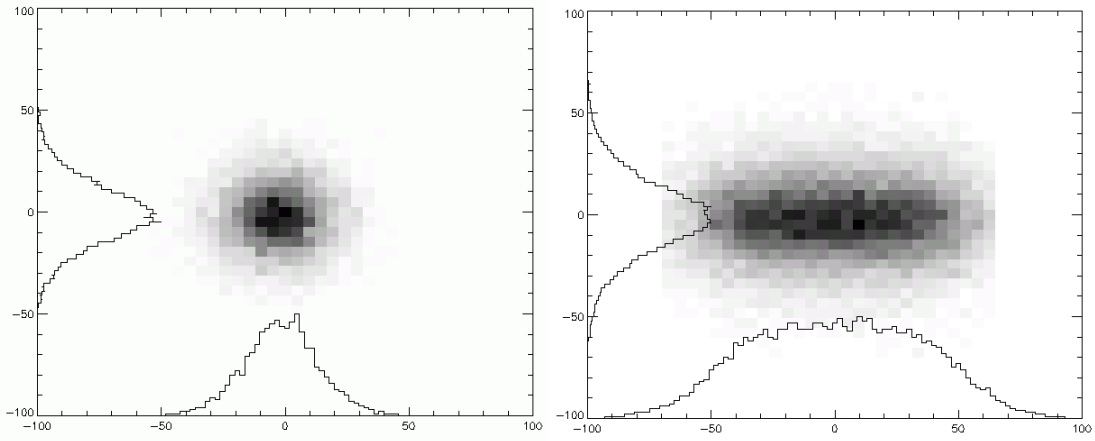

Figure 25: Monte-Carlo simulation. Simulated signal on the top surface of the cloud. The grey value is proportional to the radiance. Left: Point source; Right: Horizontal line source extended along the x-axis. The source height was 7 km below cloud top. (Note, the number on the axis description have to be divided by 3 in order to get distances in km.)

Shape of the distribution For positions well inside the cloud, the outcoming radiation distribution can be well described by a circular normal distribution centred at the horizontal position of the source point (x_0, y_0):

$$I(x, y) = A(z_0) \exp\left[-\frac{(x - x_0)^2 + (y - y_0)^2}{2\sigma(z_0)^2}\right] \tag{22}$$

with amplitude $A(z_0)$ and σ - the standard deviation, which describes the spreading of the radiation. The total energy is $I_{up} = 2\pi\sigma(z_0)^2 A(z_0)$, it depends on the source energy and the vertical position as shown below.

For normal distributions all higher cumulants except mean and variance are zero (see e.g. Feller, 1991). Hence the *kurtosis excess* is a good parameter to describe deviation from the normal distribution. The kurtosis excess is defined as

$$\kappa_4 \equiv \frac{\mu_4}{\sigma^4} - 3 \tag{23}$$

with μ_4 - 4th central moment and σ - standard deviation. For source point locations closer to the cloud surface we found increasing values of κ_4, that means the distribution is sharper in the center and falls slower at the tails compared with a normal distribution (where $\kappa_4 = 0$).

The standard deviation scales with the distance as shown on Figure 26. From the simulations we found the scaling law $\sigma = b \cdot z^a$ with exponent 0.25 for the larger distances, while for the smaller distances the best fit yield an exponent $a = 0.36$ (for $z < 8\lambda_e$, i.e. 4 km for $\lambda_e = 0.5$ km).

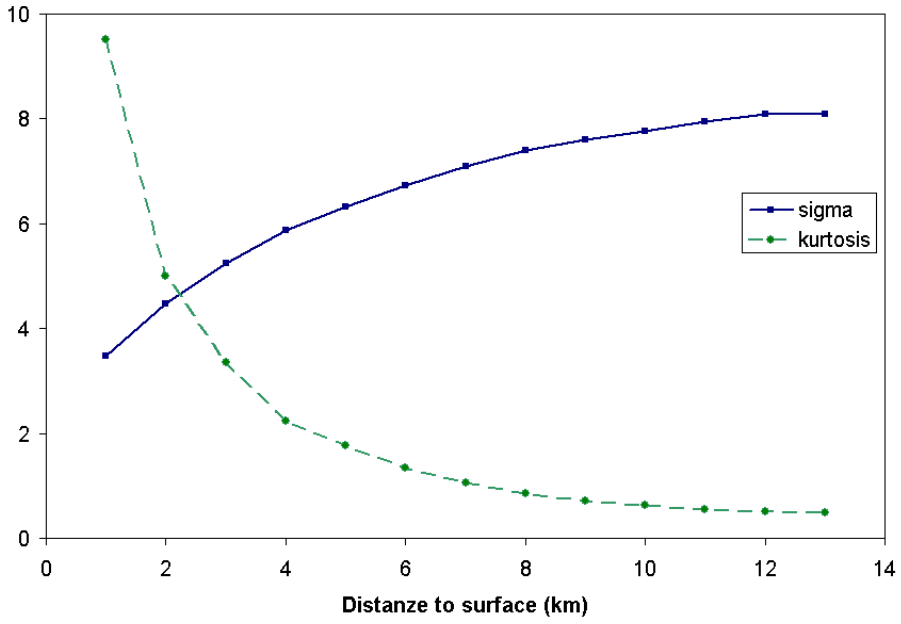

Figure 26: Monte-Carlo simulation. Dependence of sigma on the vertical distance between source and upper cloud surface. The broken line shows the kurtosis excess, i.e. the deviation from normal

Partitioning between upper and lower surface The partitioning of the photons between the upper and the lower cloud surface was found to be a linear function of vertical distance between source and surface.

$$I_{up} = \frac{z_0 - z_{dn}}{z_{up} - z_{dn}} I_0 \tag{24}$$

This is valid unless the distance becomes closer than appr. $2\lambda_e$.

Source below the cloud If the source point is below the cloud then the 1/2 of the source energy is radiated downward immediately without scattering. This part is lost to the ground. The upward radiated energy is attenuated according to a spherical wave until it reaches the cloud bottom. If the source point is at a vertical distance d below the cloud, the radiation field arriving at the lower cloud surface is described by:

$$I(x,y) = \frac{I_0}{2\pi} \frac{d}{d^2 + (x - x_0)^2 + (y - y_0)^2} \tag{25}$$

From this starting position the most part is scattered downward and only a small fraction of the source energy arrives at the upper surface with a large spreading.

For a source position 1 km below the cloud base we found by simulation for the distribution at the upper cloud surface a $\sigma \approx 13$ km. Only a partition of 3% from the starting photons was scattered finally to the upper cloud surface.

Path length and time delay The source was a delta impulse in time. Due to the different travel lengths the photons arrive at the surface with different time delay. This leads to a broadening of the impulse in time. Figure 27 shows the broadening of the impulse for a source location at 8 km distance from the cloud top. The time delay of the photons show a broad distribution from 40 μs to 3 ms.

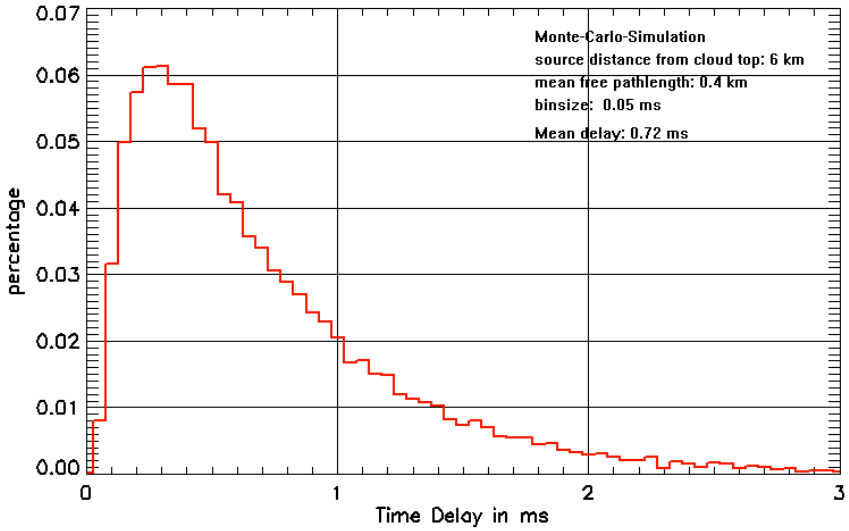

Figure 27: Distribution of the time delay after scattering for photons which were released at 8 km vertical distance to the cloud upper surface. This figure shows the variation in time of the optical signal which would be received by a detector.

Mean delay is 0.72 ms. The corresponding mean path length of the photons is 216 km. This graph is comparable to the optical wave forms detected by the photo diode of the FORTE satellite (Light et al., 2001).

10.4.2 Superposition for extended sources

For extended lightning channels the results from the point source can be simply superposed. Then for the following quantities holds:

Total upwelling radiance The amount of the total upwelling radiation I_{up} does not depend on the details of the source the geometry and orientation of the source points. It depends only on the vertical position of the 'center of energy' of the source point distribution, i.e. the average of the vertical positions weighted by the emission energy. Hence I_{up} can be expressed by

$$I_{up} = \frac{\langle z \rangle - z_{dn}}{z_{up} - z_{dn}} \cdot I_0 \tag{26}$$

with I_0 - the total emission energy and $\langle z \rangle$ - the vertical position of the 'center of energy' of the lightning source:

$$\langle z \rangle \equiv \frac{\sum_i z_{0,i} I_{0,i}}{\sum_i I_{o,i}} \tag{27}$$

Particularly this means, that horizontal lightning will give the same total upwelling radiation as vertical lightning of the same length, mean position and total source energy.

Geometrical pattern of the distribution is the sum of circular normal distributions each centred above the corresponding source point as given by (22).

$$R(x, y) = \sum_i I_i(x, y; x_{0,i}, y_{0,i}, z_{0,i}) \tag{28}$$

This can be done numerically or analytically depending on the source distribution. An example for a horizontal line source is displayed on Figure 25.

10.5 Summary of the simulation results

The following main qualitative results from the model simulations with a plane cloud:

1. The surface distributions from point sources are circular symmetric and can be well approximated by a circular normal distribution with standard deviation depending on the distance between the point source and cloud surface.
2. The vertical position if the lightning source in cloud determines the partitioning of the energy between the upper and the lower surface. This partition depends linearly on the vertical distance.
3. Lightning below the cloud is attenuated much more, only a small partition arrives at the upper cloud surface. This concerns the lightning return strokes between cloud and ground, a large part of which is below the cloud. However, since the optical energy from return strokes is usually much larger than for intracloud lightning it can be expected, that the contribution from cloud-to-ground return strokes should bee seen on the upper cloud surface as well.
4. The vertical orientation of the lightning channel inside the cloud does not affect the total radiation coming to the upper surface. The only important parameter is the mean vertical distance of the channel to the cloud surface.

5. For sources close to the cloud surface (closer than $\approx 4\lambda_e$, the effective free path length) the deviations from the normal distributions are larger. In these cases, the assumption of optically thick cloud is violated and the isotropic diffusion approximation can not be applied. For these cases the anisotropic phase function (e.g. (19)) should be used in the Monte-Carlo simulation.
6. The radiation direction direction is isotropic at the upper surface, hence the model represents the cloud as a Lambertian surface.

10.5.1 Conclusions

The developed model simulates the light transport from the lightning source to the outer surface of the cloud in a satisfactory manner. The resulting radiance pattern on the upper cloud surface can be retrieved as well as the outcoming radiance direction, the shape and delay of the optical pulse. Also the partition of energy between the various cloud surfaces and the impact of the position of the lightning source can be studied.

The model was used here for a plane plate cloud, but it is not confined to this simple case. Other cloud geometries can be introduced as well, merely the conditions for the exit of the photons out of the cloud have to be changed.

A further application of the model could be the study of different cloud ensembles, e.g. high convective clouds with a certain distribution of lightning sources.

10.5.2 Deliverable

The Monte-Carlo model is deliverable as documented source code and can be utilized for simulation of photon transport. The input parameters are the cloud dimensions, the scattering parameters (free path length and asymmetry parameter) and the source geometry and emission strength (see description in section 10.3.1.

The output is the distribution of exit locations and directions, the energy distribution, total path length and number of scattering events.

11 Summary and conclusion

This study was aimed to give a description of the lightning source characteristics as it is observed by optical means from above the clouds. These characteristics were determined from statistical analyses of the data set produced by the satellite based LIS sensor from NASA.

The frequency distribution of lightning events and their clustering in time and space was determined for the small scales. Most of the lightning events were single events, which is typical for a part of intracloud lightning. Lightning flashes consisting of several single strokes had duration mostly inside 1 s, which is also observed in ground based observations of cloud-to-ground lightning.

For the optical radiance from lightning it was found, that faint lightning is the most frequent. The radiation distribution function falls off exponentially with radiance amplitude. On the other hand, lightning is clustered and autocorrelated for short times. Hence many of the weak events are accompanied by larger amplitude events. This was shown for the flash data which consist of many single

lightning events. It was found that for 90% of all flashes contain events with radiance amplitudes larger than $10\,\mu\mathrm{J\,m^{-2}\,sr^{-1}}$.

The background radiation from the clouds was found to be large during the day time mostly larger than the lightning signal. As expected the background radiance scales well with the solar zenith angle. Lightning is mostly found in the brightest clouds for a given solar zenith angle. Due to the high background radiance the signal to signal plus noise ratio is unfavourable, mostly below 0.5 during the day time. Hence a elaborated algorithm is necessary to discriminate the lightning signal from the background.

The derived statistical results were transformed briefly to the prospected geostationary observation geometry. The field of view is considerably larger, hence more lightning data will arrive at the same time. A mean lightning event rate of $40\,\mathrm{s^{-1}}$ was estimated. Another effect is the 'horizon brightening' due to the larger pixel footprint area in the outer parts of the visible disk with the highest satellite zenith angles. This leads to enhanced background radiance but will also enhance the lightning signal.

12 Outlook

The provided statistics is not complete, the comprehensive data set allows for many additional studies and analyses.

Using the distribution of the parameters, particularly the radiance, various scenarios can be studied in order to model the detection efficiency and the false alarm rate according to possible sensor characteristics such as pixel size, pixel detection threshold and others.

A 'lightning data generator' can be developed, which output are random events with time, position and radiance having the same statistical distribution as was found in this study. This can be done in combination with the modelling of the background radiation from clouds in dependence on time and geographic position.

In addition to the presented study also other optical lightning data can be used for comparison. The full disk Meteosat visible data can be analysed in more detail in order a more complete picture of the distribution of the background radiance, using additionally the infrared data for cloud recognition.

The scattering simulation demonstrated useful results despite its high simplification. A further developing and refinement of the Monte-Carlo model should give better quantitative results for the radiance distribution for the various properties of clouds and lightning source.

Acknowledgements

We acknowledge gracefully the provision of the LIS and OTD data by NASA MSFC and the German Weather Service (DWD).

References

Boccippio, D., W. Koshak, R. Blakeslee, K. Driscoll, D. Mach, W. Boeck, H. Christian, and S. Goodman (2000). The Optical Transient Detector (OTD): Instrument characteristics and cross-sensor validation. *J. Atmos. Oceanic Technol. 17*, 441–458.

Boccippio, D. J., K. Driscoll, J. Hall, and D. Buechler (1998). LIS/OTD Software Guide. Technical report, Global Hydrology and Climate Center, NASA. 127 pp.

Boccippio, D. J., W. J. Koshak, and R. J. Blakeslee (2002). Performance assessment of the optical transient detector and lightning imaging sensor. Part I: Predicted diurnal variability. *J. Atmos. Oceanic Technol. 19*, 1318–1332.

Christian, H. J., R. J. Blakeslee, D. J. Boccippio, W. L. Boeck, D. E. Buechler, K. T. Driscoll, S. J. Goodman, J. M. Hall, W. J. Koshak, D. M. Mach, and M. F. Stewart (2003). Global frequency and distribution of lightning as observed from space by the optical transient detector. *J. Geophys. Res. 108*, 4005, doi:10.1029/2002JD002347.

Christian, H. J., R. J. Blakeslee, and S. J. Goodman (1989). The detection of lightning from geostationary orbit. *J. Geophys. Res. 94*, 13,329–13,337.

Christian, H. J., R. J. Blakeslee, S. J. Goodman, and D. M. Mach (1995). Algorithm theoretical basis document (ATBD) for the lightning imaging sensor (LIS). Technical report, NASA/Marshall Space Flight Center. 51 pp.

Christian, H. J. and S. J. Goodman (1987). Optical observations of lightning from a high-altitude airplane. *J. Atmos. Oceanic Technol. 4*, 701–711.

Davis, A. B. and A. Marshak (2002). Space-time characteristics of light transmitted through dense clouds: A Green's function analysis. *J. Atmos. Sci. 59*, 2713–2727.

Dyudina, U. A., A. P. Ingersoll, A. R. Vasavada, and S. P. Ewald (2002). Monte Carlo radiative transfer modeling of lightning observed in Galileo images of Jupiter. *Icarus 160*, 336–349.

Feller, W. (1991). *An Introduction to Probability Theory and Its Applications*. John Wiley & Sons. 669 pp.

Koshak, W. J., R. J. Solakiewicz, D. D. Phanord, and R. J. Blakeslee (1994). Diffusion model for lightning radiative transfer. *J. Geophys. Res. 99*, 14,361–14,371.

Koshak, W. J., M. F. Stewart, H. J. Christian, J. W. Bergstrom, J. M. Hall, and R. J. Solakiewicz (2000). Laboratory calibration of the optical transient detector and the lightning imaging sensor. *J. Atmos. Oceanic Technol. 17*(7), 905–915.

Light, T. E., D. M. Suszcynsky, M. W. Kirkland, and A. R. Jacobson (2001). Simulations of lightning optical waveforms as seen through clouds by satellites. *J. Geophys. Res. 106*, 17,103–17,114.

Mach, D. M., R. Blakeslee, J. Bailey, W. Farrell, R. Goldberg, M. Desch, and J. Houser (2003). Preliminary optical and electric field pulse statistics from storm overflights during the Altus cumulus electrification study. In *12th International Conference on Atmospheric Electricity*, June 9-13, Versailles, France.

Prahl, S., M. Keijzer, S. L. Jacques, and A. J. Welch (1989). A Monte Carlo modeling of light transport in tissue. In G. Mueller and D. Sliney (Eds.), *Dosimetry of Laser Radiation in Medicine and Biology*, SPIE Institute Series Vol. IS 5, pp. 102–111. SPIE.

Thomason, L. W. and E. P. Krider (1982). The effects of clouds on the light produced by lightning. *J. Atmos. Sci. 39*, 2051–2065.

List of Figures

Appendix

A Monte-Carlo Model Description

For the implementation of a Monte-Carlo model we adapted the method used in Prahl et al. (1989) for light propagation simulation in tissue. The model simulates a random walk in 3 dimensions for a large number of photons (e.g. 10^5). The direction changes during the random walk are due to scattering according to the phase function. Between the scattering events the photons move with constant velocity vector. Scattering is modelled with the HG-phase function. The series of path lengths between the scattering events and the scattering angles are random deviates. After the photon crossed the cloud surface it escapes the cloud, no more scattering takes place from this point.

The random scattering parameters for each photon are generated starting with a vector of uniform random numbers $r \in (0, 1)$. Using generating functions this vector is transformed into random variables which satisfy the desired distribution law. For the gamma distributed path lengths s we use the

generating function:

$$s = -\ln(r) \cdot \langle \lambda_e \rangle \tag{29}$$

The series of scattering angles (θ_m), i.e. the deflection angle from the actual direction, is generated using the generating function for the Henyey-Greenstein-function (19):

$$\cos\theta = \frac{1}{2g}\left[1 + g^2 - \left(\frac{1-g^2}{1+g(2r-1)}\right)^2\right] \tag{30}$$

For isotropic scattering, i.e. $g = 0$, the generating function (30) simplifies to

$$\cos\theta = 2r - 1 \tag{31}$$

The scattering azimuth angles are uniformly distributed between $(0, 2\pi)$:

$$\phi = 2\pi r \tag{32}$$

An weak absorption can be incorporated, e.g. by giving every scatter event a small probability of killing the photon. Hence the output would contain less 'long travelling' photons.

The propagation of the photons from the old to the new position can be expressed simply by the direction cosines (μ_x, μ_y, μ_z) which are defined as the cosines of the angle of the direction to the Cartesian axes. The new positions calculate as:

$$\begin{aligned} x' &= x + \mu'_x \cdot s \\ y' &= y + \mu'_y \cdot s \\ z' &= z + \mu'_z \cdot s \end{aligned} \tag{33}$$

At each scattering point the new direction cosines are calculated from the random generated scattering angles θ (according to (30) or (31)) and the uniform distributed ϕ as:

$$\begin{aligned} \mu'_x &= \frac{\sin\theta}{\sqrt{1-\mu_z^2}}(\mu_x\mu_z\cos\phi - \mu_y\sin\phi) + \mu_x\cos\theta \\ \mu'_y &= \frac{\sin\theta}{\sqrt{1-\mu_z^2}}(\mu_y\mu_z\cos\phi + \mu_x\sin\phi) + \mu_y\cos\theta \\ \mu'_z &= -\sin\theta\cos\phi\sqrt{1-\mu_z^2} + \mu_z\cos\theta \end{aligned} \tag{34}$$

for angles close to the vertical $|\mu_z| \approx 1$ it reduces to

$$\begin{aligned} \mu'_x &= \sin\theta\cos\phi \\ \mu'_y &= \sin\theta\sin\phi \\ \mu'_z &= \mathrm{sign}(\mu_z)\cos\theta \end{aligned} \tag{35}$$

For each of the photons the random walk path is generated with a large number of single steps ($M > 1500$, usually). Then the random walk path is examined and the position ($\vec{r}_{n,e}$) and direction ($\vec{\mu}_{n,e}$) at the exit point of the cloud is determined. Additionally the number of scattering events (n_n) and the total path length (L_n) of the photon inside cloud is stored.

The starting distribution ($\vec{r}_{n,0}, \vec{\mu}_{n,0}$) is set along the lightning channel source with random emission angles.

B Abbreviations

CCD	Charge Coupled Device
DE	Detection Efficiency
FORTE	Fast On-orbit Recording of Transient Events
FOV	Field of View
GEO	Geostationary Orbit
HDF	Hierarchical Data Format
IDL	Interactive Data Language
LANL	Los Alamos National Laboratory
LIS	Lightning Imaging Sensor
LST	Local Solar Time
MSFC	Marshall Space Flight Center of NASA in Huntsville, Al
NASA	National Aeronautic and Space Administration
OTD	Optical Transient Detector
SZA	Solar Zenith Angle
TRMM	Tropical Rainfall Measurement Mission